Research Square

Preprints are preliminary reports that have not undergone peer review.
They should not be considered conclusive, used to inform clinical practice,
or referenced by the media as validated information.

Implementation of the Quantum Fourier Transform in Quantum Optical Processors Using Linear Optics with Imperfect Circuits

Mohammad Bayat
Arak University
Mehran Gholipour Shahraki
Arak University
Mehdi Mirzaee
M-mirzaee@araku.ac.ir
Arak University

Article

Keywords: Quantum Fourier Transform, Linear optical devices, Cooley-Tukey algorithm, Qubit states

Posted Date: August 26th, 2026

DOI: https://doi.org/10.21203/rs.3.rs-10522134/v1

License: This work is licensed under a Creative Commons Attribution 4.0 International License.
Read Full License

Additional Declarations: No competing interests reported.

Implementation of the Quantum Fourier Transform in Quantum Optical Processors Using Linear Optics with Imperfect Circuits

Mohammad Bayat[1], Mehran Gholipour Shahraki[1,2], Mehdi Mirzaee[1*]

[1*]Department of Physics, Faculty of Science, Arak University, Arak, 384817758, Iran.
[2]Institute of Nanoscience & Nanotechnology, Arak University, Arak, Iran.

*Corresponding author(s). E-mail(s): M-mirzaee@araku.ac.ir;
Contributing authors: Msbayat2000@gmail.com;
M-gholipour@araku.ac.ir;

Abstract

This paper investigates the implementation of the Quantum Fourier Transform (QFT) using linear optical devices and the Cooley-Tukey algorithm, with a focus on the impact of device imperfections and phase errors due to optical path differences. It examines real-world defects in optical gate circuits, systematically analyzing these imperfections for systems with two, three, and general γ-qubit states, providing a comprehensive formula for the γ-qubit case.

Keywords: Quantum Fourier Transform, Linear optical devices, Cooley-Tukey algorithm, Qubit states

1 Introduction

In 1981, Richard Feynman, during a lecture, questioned whether classical computers could effectively solve real-world problems involving quantum mechanics. He argued that such problems often require numerically approximating differential equations, a task that classical computers struggle to handle accurately [1]. Feynman proposed that solving quantum mechanical problems would require a new type of computer, one that

operates according to the principles of quantum mechanics, as classical computers are fundamentally incapable of providing accurate and realistic solutions.

Since then, several physical platforms have been proposed and developed for building quantum computers. Among the most prominent are trapped ions and superconducting circuits. Trapped ion systems use ions confined by electromagnetic fields as qubits, benefiting from long coherence times and high-fidelity gate operations. However, they face challenges related to scalability, as controlling and coupling many ions becomes increasingly complex [2]. Superconducting qubits, on the other hand, operate at microwave frequencies and offer fast gate times and easier integration with existing electronics, yet suffer from shorter coherence times and fabrication variability [3].

Despite significant progress, these approaches face substantial hurdles in scalability, error correction, and operational stability, which slow down their path toward large-scale quantum computing.

Photonic qubits, which encode quantum information in properties of individual photons such as polarization or path, offer several advantages compared to trapped ions and superconducting circuits. Photons naturally travel at the speed of light and interact weakly with their environment, resulting in very low decoherence rates and the ability to transmit quantum information over long distances with minimal loss. Furthermore, photonic systems can operate at room temperature, reducing the need for complex cryogenic setups required by superconducting qubits. Additionally, the integration of photonic components with existing fiber-optic communication infrastructure makes photonic qubits a promising candidate for scalable quantum networks and distributed quantum computing. However, challenges remain in creating deterministic two-qubit gates and generating on-demand single photons with high efficiency [4].

To address some of these challenges, researchers have explored quantum computing architectures based entirely on linear optical elements. Optical components such as beam splitters, phase shifters, and interferometers—well-established in classical photonics—can be used to implement quantum logic gates and manipulate photonic qubits with high precision. Foundational results have shown that any arbitrary unitary operation can be decomposed into a network of such optical elements [5–7]. These capabilities, combined with advances in integrated photonics and single-photon sources, are paving the way for compact, scalable, and room-temperature quantum computing platforms based on optics.

Further foundational work by Reck and Zeilinger established that any $N \times N$ unitary transformation could be decomposed into a sequence of beam splitters and phase shifters, providing a universal toolkit for optical quantum circuits [7]. These theoretical and experimental breakthroughs laid the groundwork for the rapid development of integrated photonic platforms, which aim to implement large-scale quantum circuits on compact and scalable chips [6, 8]. Recent advances in fabrication techniques and single-photon sources have significantly improved the performance and scalability of these integrated photonic systems, making them a promising candidate for practical quantum computing implementations.

Among the landmark results in quantum computing is Shor's algorithm, which showed that quantum systems could, in principle, solve certain problems more efficiently than classical computers [9]. Central to many such algorithms is the quantum Fourier transform (QFT)[9–11], an operation that extracts periodicity information from quantum states and forms a foundational building block for a wide range of quantum computational protocols.

The QFT is especially important in optical quantum computing, where single-photon systems can be integrated with QFT techniques to enhance computational capabilities [9–37] It enables quantum processors to perform discrete Fourier transforms on quantum states, allowing solutions to problems that are currently intractable for classical approaches [12, 15]. The ongoing integration of single-photon sources with QFT and other linear optical methods continues to advance the development of scalable quantum computing platforms [5–7].

These developments bring us closer to building powerful quantum computers capable of tackling complex problems beyond the scope of classical computation [36–48] Nevertheless, challenges remain, especially in mitigating noise and errors when combining single-photon technologies with QFT and other quantum computing methods.

The primary technical challenge in scaling linear optical devices is the significant overhead required to implement multi-qubit gates. Additionally, ensuring phase stability between optical modes often demands continuous monitoring and calibration, a process that becomes increasingly complex as the circuit expands [12]. .In this paper, we investigate the impact of imperfections in beam splitters, a key component in optical quantum computing, as well as phase errors in path differences. This work proposes a new equation to account for these challenges when implementing the QFT in optical circuits.

The remainder of the paper is structured as follows: **Section 2** This section provides a brief introduction to linear optics and outlines the basic principles relevant to quantum gate implementation. Special attention is given to the Hadamard gate, including possible deviations from its ideal form. **Section3** focuses on the QFT and the Cooley-Tukey algorithm, analyzing their implementation using linear optics while addressing potential sources of error in optical devices. **Section 4** examines the effects of imperfections in two-, three-, and n-qubit systems, providing a computational analysis of how these imperfections impact optical QFT. This section concludes with a general formula for γ-qubit systems, offering a framework for managing imperfections in larger optical setups. **Section 5** provides an analysis of the phase error introduced by differences in optical path lengths. Finally, **Section 6** concludes with a summary of the findings and discusses the implications for future research in optical quantum computing.

2 linear optical devices and error

Integrated linear optics relies on fundamental components such as mirrors, phase shifters, waveguides, and beam splitters, which collectively enable the manipulation of photonic qubits [22, 23, 25]. In this work, we focus on path-encoded photonic qubits,

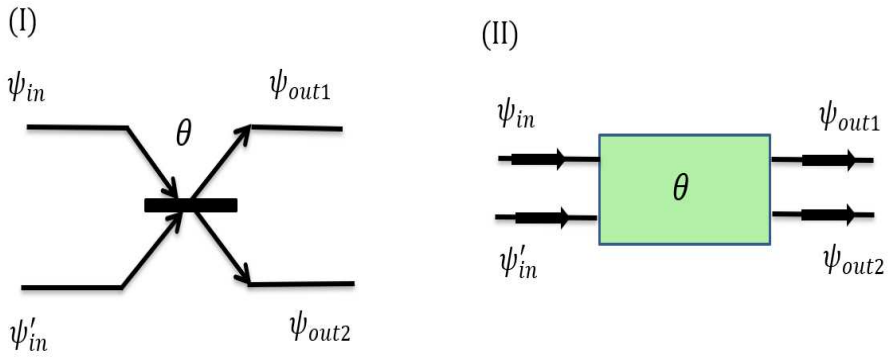


Fig. 1: (I) A beam splitter with two input and two output ports. (II) A block diagram of the beam splitter.

where the logical states $|0\rangle$ and $|1\rangle$ are represented by the presence of a single photon in one of two distinct spatial modes. This choice of encoding is particularly compatible with integrated photonic platforms and is distinct from other approaches such as polarization encoding.

In [26, 27], the connection between two input states ψ_I and two output states ψ_O of a lossless beam splitter is represented by a unitary matrix U, where $\psi_O = U\psi_I$ and $\delta_{\text{Right}} + \delta_{\text{Left}} = \pi$, with δ representing the phase shift between the transmitted and reflected waves (see Fig. 1).

Furthermore, [25] demonstrates that a beam splitter combined with two $-\frac{\pi}{2}$ phase shifters can function as a Hadamard gate [15, 48]:

$$U = H = \frac{1}{\sqrt{2}} \begin{pmatrix} 1 & 1 \\ 1 & -1 \end{pmatrix} \tag{1}$$

However, imperfections in fabrication and alignment often lead to unbalanced beam splitting, which disturbs the ideal transformation. This effect can be modeled using a non-ideal Hadamard gate, parameterized by a splitting angle θ, given by [25]:

$$H(\theta) = \begin{pmatrix} \cos\frac{\theta}{2} & \sin\frac{\theta}{2} \\ \sin\frac{\theta}{2} & -\cos\frac{\theta}{2} \end{pmatrix} \tag{2}$$

This generalized form accounts for deviations in the beam splitter's reflectivity and transmissivity, capturing one of the key sources of error in linear optical quantum circuits. Another source of error arises from phase shifts introduced by differences in optical path lengths. These are modeled by the unitary operator $L(L_1, L_2)$, which represents the relative phase difference acquired by a photon traveling along two distinct optical paths with lengths L_1 and L_2, respectively:

$$L(L_1, L_2) = \begin{pmatrix} e^{\frac{2\pi i L_1}{\lambda}} & 0 \\ 0 & e^{\frac{2\pi i L_2}{\lambda}} \end{pmatrix} \tag{3}$$

Here, λ denotes the wavelength of the incoming photon, and L_1, L_2 represent the respective optical path lengths. These models enable a precise analysis of physical

imperfections affecting photonic implementations of quantum algorithms, such as the QFT, within integrated optical circuits.

3 Discrete and Quantum Fourier Transforms

The Discrete Fourier Transform (DFT) is a fundamental tool that converts a discrete sequence from its original domain into the frequency domain. Given a complex input sequence $y_0(k)$ of length N, its DFT $Y(n)$ is defined as [13, 14]:

$$Y(n) = \sum_{k=0}^{N-1} y_0(k) \exp\left(-i2\pi \frac{kn}{N}\right) = \sum_{k=0}^{N-1} y_0(k) M^{nk}, \quad n = 0, 1, \ldots, N-1, \tag{4}$$

where

$$M = \exp\left(-i\frac{2\pi}{N}\right),$$

and N is the length of the input sequence.

Here, $y_0(k) \in \mathbb{C}$ is the input discrete sequence, and $Y(n) \in \mathbb{C}$ is its corresponding DFT output. Moreover:

- $y_0(k)$ is a discrete sequence of complex values: $y_0(k) \in \mathbb{C}$,
- $Y(n)$, which is the DFT of $y_0(k)$, is also a complex sequence: $Y(n) \in \mathbb{C}$,
- $y(n)$, which represents the signal in the time domain, is also assumed to be complex by default.

Computing the DFT directly from the definition requires $O(N^2)$ operations, which can be computationally expensive for large N. The Fast Fourier Transform (FFT) is an efficient family of algorithms that significantly reduce this computational cost to $O(N \log N)$ by exploiting the symmetries and periodicities in the DFT [16, 17]. One of the most prominent FFT algorithms is the Cooley-Tukey method [16]. This recursive divide-and-conquer algorithm factors a DFT of composite size $N = N_1 N_2$ into smaller DFTs of sizes N_1 and N_2. By repeatedly breaking down the problem, it dramatically reduces the number of computations. Moreover, the Cooley-Tukey algorithm is quite general and can handle input sizes N that factor into arbitrary integers.

A widely used special case of the Cooley-Tukey algorithm is the Radix-2 FFT, which applies when the input size N is a power of two [17]. In this case, the input sequence is recursively split into halves until sequences of length two are reached, enabling a simple and efficient implementation. The recursive nature of the Radix-2 FFT aligns well with the structure of the QFT, which similarly relies on decomposing the transform into smaller components [18].

The Radix-2 FFT requires that

$$N = 2^\gamma, \quad \gamma \in \mathbb{Z}^+,$$

which facilitates the recursive decomposition of the DFT into transforms of size 2. This property is a key feature leveraged in quantum algorithms based on the QFT [18, 19].

In an n-qubit quantum system with computational basis states

$$\{|X(n)\rangle\} = \{|X_0\rangle, |X_1\rangle, \ldots, |X_{N-1}\rangle\},$$

the Quantum Fourier Transform (QFT) maps each basis state $|X(n)\rangle$ into a superposition of all other basis states as follows:

$$|X(n)\rangle \longrightarrow \frac{1}{\sqrt{N}} \sum_{k=0}^{N-1} e^{i\frac{2\pi nk}{N}} |x_0(k)\rangle. \tag{5}$$

Equivalently, this transformation can be expressed in terms of the primitive N-th root of unity $W = e^{i\frac{2\pi}{N}}$ as:

Here, $|x_0(k)\rangle$ denotes the computational basis states of the system.

$$|X(n)\rangle \longrightarrow \frac{1}{\sqrt{N}} \sum_{k=0}^{N-1} W^{nk} |x_0(k)\rangle, \quad \text{where } W = e^{2\pi i/N}. \tag{6}$$

The QFT circuit for a two-qubit system is shown in Figure 2. The circuit begins with a Hadamard gate H applied to the most significant qubit q_0, which creates an equal superposition of its basis states. Next, a controlled-phase gate $R_2 = \mathrm{diag}(1, e^{i\pi/2})$ is applied to the least significant qubit q_1, conditioned on the state of q_0. This gate performs a phase rotation defined as:

$$R_2 = \begin{bmatrix} 1 & 0 \\ 0 & e^{2\pi i/4} \end{bmatrix} = \begin{bmatrix} 1 & 0 \\ 0 & i \end{bmatrix}. \tag{7}$$

which means it multiplies the $|1\rangle$ state of the target qubit by a phase factor of i, corresponding to a $\pi/2$ rotation in the complex plane. After applying this controlled-phase gate, a Hadamard gate is applied to q_1, generating a superposition across both qubits. Finally, a SWAP gate exchanges the two qubits. This reordering is necessary because the QFT naturally outputs the qubits in bit-reversed order compared to the classical DFT. Let the computational basis states be denoted as $|x_0(k_1, k_0)\rangle$, where (k_1, k_0) are

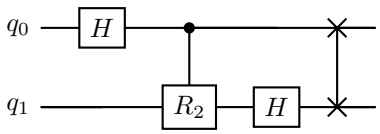


Fig. 2: QFT circuit for two qubits. It applies a Hadamard gate on q_0, a controlled-R_2 gate on q_1 (controlled by q_0), a Hadamard gate on q_1, and finally a SWAP gate to reverse the qubit order.

the binary values of the two qubits. The output of the QFT can be represented using the quantum Fourier basis states $|X(k_1, k_0)\rangle$, where the transformation coefficients are

powers of the fourth root of unity $W = e^{2\pi i/4}$. The QFT basis states are given by:

$$\begin{aligned}
|X(0,0)\rangle &= \frac{1}{\sqrt{4}}\left[W^0|x_0(0,0)\rangle + W^0|x_0(0,1)\rangle + W^0|x_0(1,0)\rangle + W^0|x_0(1,1)\rangle\right], \\
|X(0,1)\rangle &= \frac{1}{\sqrt{4}}\left[W^0|x_0(0,0)\rangle + W^1|x_0(0,1)\rangle + W^2|x_0(1,0)\rangle + W^3|x_0(1,1)\rangle\right], \\
|X(1,0)\rangle &= \frac{1}{\sqrt{4}}\left[W^0|x_0(0,0)\rangle + W^2|x_0(0,1)\rangle + W^4|x_0(1,0)\rangle + W^6|x_0(1,1)\rangle\right], \\
|X(1,1)\rangle &= \frac{1}{\sqrt{4}}\left[W^0|x_0(0,0)\rangle + W^3|x_0(0,1)\rangle + W^6|x_0(1,0)\rangle + W^9|x_0(1,1)\rangle\right].
\end{aligned} \tag{8}$$

This transformation can be expressed in matrix form as:

$$\begin{pmatrix} |X(0,0)\rangle \\ |X(0,1)\rangle \\ |X(1,0)\rangle \\ |X(1,1)\rangle \end{pmatrix} = \frac{1}{\sqrt{4}} \begin{pmatrix} W^0 & W^0 & W^0 & W^0 \\ W^0 & W^1 & W^2 & W^3 \\ W^0 & W^2 & W^4 & W^6 \\ W^0 & W^3 & W^6 & W^9 \end{pmatrix} \begin{pmatrix} |x_0(0,0)\rangle \\ |x_0(0,1)\rangle \\ |x_0(1,0)\rangle \\ |x_0(1,1)\rangle \end{pmatrix} \tag{9}$$

Using modulo arithmetic ($W^{nk} \bmod 4$), the matrix simplifies to:

$$\begin{pmatrix} |X(0,0)\rangle \\ |X(0,1)\rangle \\ |X(1,0)\rangle \\ |X(1,1)\rangle \end{pmatrix} = \frac{1}{\sqrt{4}} \begin{pmatrix} 1 & 1 & 1 & 1 \\ 1 & W & W^2 & W^3 \\ 1 & W^2 & 1 & W^2 \\ 1 & W^3 & W^2 & W \end{pmatrix} \begin{pmatrix} |x_0(0,0)\rangle \\ |x_0(0,1)\rangle \\ |x_0(1,0)\rangle \\ |x_0(1,1)\rangle \end{pmatrix} \tag{10}$$

A graphical representation of the QFT process is shown in Figure 3. Each node corresponds to a quantum state at a specific stage, and each edge represents a quantum path with an associated phase factor W^n. These phase factors correspond directly to the complex exponential rotations applied during the QFT.The quantum matrix form of this stepwise computation is described in **Appendix A**.

$$\begin{pmatrix} |x_2(0,0)\rangle \\ |x_2(0,1)\rangle \\ |x_2(1,0)\rangle \\ |x_2(1,1)\rangle \end{pmatrix} = \frac{1}{\sqrt{4}} \begin{pmatrix} 1 & W^0 & 0 & 0 \\ 1 & W^2 & 0 & 0 \\ 0 & 0 & 1 & W^1 \\ 0 & 0 & 1 & W^3 \end{pmatrix} \begin{pmatrix} 1 & 0 & W^0 & 0 \\ 0 & 1 & 0 & W^0 \\ 1 & 0 & W^2 & 0 \\ 0 & 1 & 0 & W^2 \end{pmatrix} \begin{pmatrix} |x_0(0,0)\rangle \\ |x_0(0,1)\rangle \\ |x_0(1,0)\rangle \\ |x_0(1,1)\rangle \end{pmatrix} \tag{11}$$

This leads to the extended stage-wise form shown below:

$$\begin{aligned}
|x_1(n_0,k_0)\rangle &= \frac{1}{\sqrt{2}} \sum_{k_1=0}^{1} W^{2n_0k_1} |x_0(k_1,k_0)\rangle \\
|x_2(n_0,n_1)\rangle &= \frac{1}{\sqrt{2}} \sum_{k_0=0}^{1} W^{(2n_1+n_0)k_0} |x_1(n_0,k_0)\rangle \\
|\boldsymbol{X}(\boldsymbol{n_1},\boldsymbol{n_0})\rangle &= |\boldsymbol{x}_2(\boldsymbol{n_0},\boldsymbol{n_1})\rangle
\end{aligned} \tag{12}$$

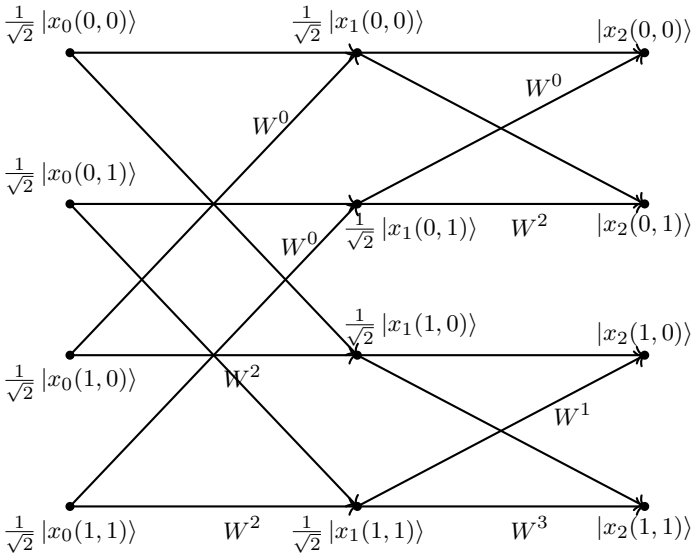


Fig. 3: Graph representation of the QFT for $N = 4$. Each arrow represents a computational path between quantum states with a complex exponential phase weight $W^n = e^{2\pi i n/4}$. This structure mirrors the recursive nature of the Cooley–Tukey FFT decomposition.

For $N = 8 = 2^3$, the same process generalizes to:

$$
\begin{aligned}
|x_1(n_0, k_1, k_0)\rangle &= \frac{1}{\sqrt{2}} \sum_{k_2=0}^{1} W^{4n_0k_2} |x_0(k_2, k_1, k_0)\rangle \\
|x_2(n_0, n_1, k_0)\rangle &= \frac{1}{\sqrt{2}} \sum_{k_1=0}^{1} W^{(2n_1+n_0)(2k_1)} |x_1(n_0, k_1, k_0)\rangle \\
|x_3(n_0, n_1, n_2)\rangle &= \frac{1}{\sqrt{2}} \sum_{k_0=0}^{1} W^{(4n_2+2n_1+n_0)k_0} |x_2(n_0, n_1, k_0)\rangle \\
|\boldsymbol{X}(\boldsymbol{n_2}, \boldsymbol{n_1}, \boldsymbol{n_0})\rangle &= |\boldsymbol{x}_3(\boldsymbol{n_0}, \boldsymbol{n_1}, \boldsymbol{n_2})\rangle
\end{aligned}
\tag{13}
$$

In the most general form, for any $N = 2^\gamma$, we have:

$$|x_1(n_0, k_{\gamma-2}, k_{\gamma-3}, \ldots, k_0)\rangle = \frac{1}{\sqrt{2}} \sum_{k_{\gamma-1}=0}^{1} W^{2^{\gamma-1} n_0 k_{\gamma-1}} |x_0(k_{\gamma-1}, k_{\gamma-2}, \ldots, k_0)\rangle$$

$$|x_2(n_0, n_1, k_{\gamma-3}, \ldots, k_0)\rangle = \frac{1}{\sqrt{2}} \sum_{k_{\gamma-2}=0}^{1} W^{(2n_1+n_0)2^{\gamma-2} k_{\gamma-2}} |x_1(n_0, k_{\gamma-2}, \ldots, k_0)\rangle$$

$$\vdots$$

$$|x_\gamma(n_0, n_1, \ldots, n_{\gamma-1})\rangle = \frac{1}{\sqrt{2}} \sum_{k_0=0}^{1} W^{(2^{\gamma-1} n_{\gamma-1} + \cdots + 2n_1 + n_0) k_0} |x_{\gamma-1}(n_0, n_1, \ldots, k_0)\rangle$$

$$|\boldsymbol{X}(\boldsymbol{n_{\gamma-1}}, \ldots, \boldsymbol{n_0})\rangle = |\boldsymbol{x}_\gamma(\boldsymbol{n_0}, \ldots, \boldsymbol{n_{\gamma-1}})\rangle \tag{14}$$

This recursive representation describes the quantum formulation of the Cooley–Tukey Fast Fourier Transform, applicable for any $N = 2^\gamma$, where γ is the number of stages (or the depth of recursion).

Moreover, any unitary operation in an N-dimensional Hilbert space can be decomposed into a sequence of $\frac{N(N-1)}{2}$ beam splitter (BS) operations. This represents the upper bound on the number of beam splitters required to implement a general unitary transformation [7]. Furthermore, it has been shown that any γ-qubit unitary transformation can be implemented using at most $2^{\gamma-1}(2^\gamma - 1)$ combinations of BS and phase shifters (PS) [24].

The Cooley-Tukey algorithm improves this decomposition by factorizing a $2^\gamma \times 2^\gamma$ unitary matrix into $\gamma \cdot 2^{\gamma-1}$ qubit transformations, which can be implemented using linear optics through BS and PS. More precisely, the Cooley-Tukey algorithm decomposes a $2^\gamma \times 2^\gamma$ unitary matrix into γ successive stages, each consisting of $2^{\gamma-1}$ unitary transformations [15].

Based on the above considerations, in this paper, we adopt the Cooley-Tukey algorithm for implementing the QFT. The key advantage of using this algorithm lies in its recursive structure, which significantly reduces the overall complexity of the transformation. It allows for efficient hardware implementation using a reduced number of optical elements, particularly beam splitters and phase shifters, which makes it highly suitable for photonic quantum computing platforms. Furthermore, the modular nature of the Cooley-Tukey decomposition facilitates scalability and parallelization, which are essential for practical realizations of large-scale quantum circuits.

4 Implementation of OQFT in Imperfect Circuits

When the QFT is realized using optical components, it is referred to as the Optical Quantum Fourier Transform (OQFT). In this implementation, each node in the DFT corresponds to a beam splitter (BS), and the connections between nodes represent optical waveguides guiding single photons.

In this section, we investigate the impact of device imperfections on the performance of OQFT circuits. We begin by analyzing a two-qubit OQFT system, followed by the extension to a three-qubit system. Finally, a general γ-qubit system is considered, and a new formula is proposed to quantify and mitigate the effects of imperfections.

As analyzed in **Section 2**, a beam splitter with imperfections can be modeled by deviations in its characteristic parameters. In an ideal beam splitter, where the parameter $\theta = \frac{\pi}{2}$, the transfer matrix is given by

$$H\left(\theta = \frac{\pi}{2}\right) = \begin{pmatrix} \frac{1}{\sqrt{2}} & \frac{1}{\sqrt{2}} \\ \frac{1}{\sqrt{2}} & -\frac{1}{\sqrt{2}} \end{pmatrix}. \tag{15}$$

This matrix represents a perfect 50:50 beam splitter that equally splits the input optical modes with the correct phase relations.

In practical scenarios, however, deviations from the ideal splitting ratio, insertion losses, and phase errors occur. Such imperfections can be incorporated by replacing θ with $\theta = \frac{\pi}{2} + \delta\theta$, where $\delta\theta$ represents a small perturbation parameter characterizing the imperfection.

Therefore, the imperfect beam splitter matrix becomes

$$H(\theta) = \begin{pmatrix} \cos\theta & \sin\theta \\ \sin\theta & -\cos\theta \end{pmatrix}, \quad \text{with} \quad \theta = \frac{\pi}{2} + \delta\theta. \tag{16}$$

In the following subsections, we analyze how these imperfections affect the fidelity and output states of OQFT circuits for two and three qubits. Subsequently, we generalize these results to an arbitrary γ-qubit system and propose correction methods to compensate for errors. However, under real conditions, perfect transmission does not occur, and unbalanced wave splitting may take place. In the following subsections (1 to 3), imperfect circuits with different qubit inputs are considered.

4.1 Two-Qubit System

It is worth noting that, in the case of a single qubit, the QFT reduces exactly to a Hadamard gate, as also discussed in Tabia [12].

To analyze a two-qubit system, two approaches can be taken. The first approach considers each beam splitter individually, solving the problem step by step. The second approach treats the entire system as a matrix; the system's matrix representation is derived first and then used to compute the output for a given input.

In the following sections, each beam splitter will first be examined separately to understand its individual contributions, and then the matrix representing the entire system will be constructed. This will allow a comprehensive analysis of the system and facilitate computation of the output from the input.

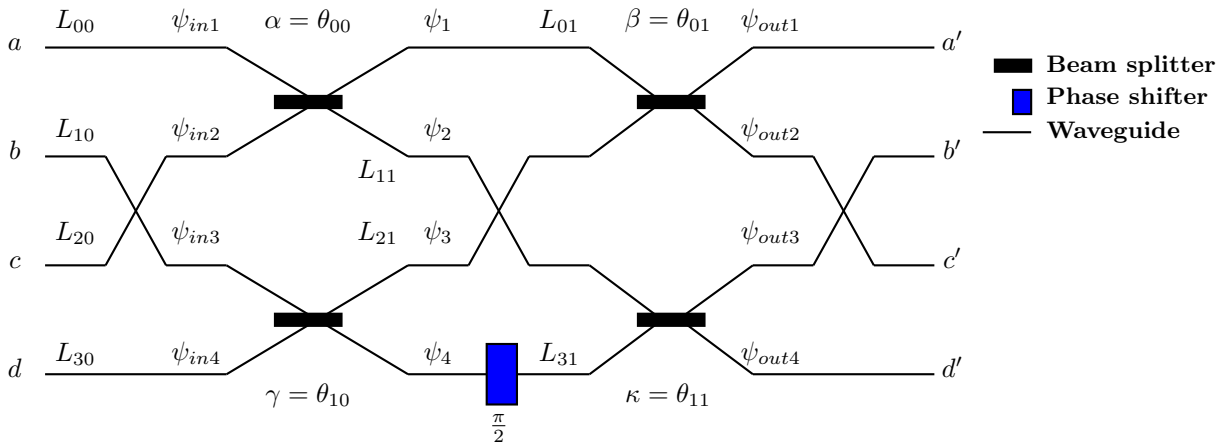


Fig. 4: A two-qubit optical circuit [12], where a, b, c, and d represent the input modes, and a', b', c', and d' are the corresponding output modes.

4.1.1 Individual Analysis of Beam Splitters

The circuit implementing a two-qubit system is shown in Fig. 4. This circuit has four inputs, a, b, c, d, and four outputs, a', b', c', d'. Because the circuit is symmetric, the parameters can be interchanged accordingly.

The outputs of the first beam splitter in the first stage, with parameter α, are ψ_1 and ψ_2:

$$\begin{pmatrix} \psi_1 \\ \psi_2 \end{pmatrix} = \begin{pmatrix} \cos\frac{\alpha}{2} & \sin\frac{\alpha}{2} \\ \sin\frac{\alpha}{2} & -\cos\frac{\alpha}{2} \end{pmatrix} \begin{pmatrix} a \\ c \end{pmatrix} = \begin{pmatrix} \cos\frac{\alpha}{2}a + \sin\frac{\alpha}{2}c \\ \sin\frac{\alpha}{2}a - \cos\frac{\alpha}{2}c \end{pmatrix} \tag{17}$$

Here, the matrix represents the transformation of the input modes a and c by the beam splitter characterized by the parameter α.

Similarly, the output of the second beam splitter in the first stage, with parameter γ, yields ψ_3 and ψ_4:

$$\begin{pmatrix} \psi_3 \\ \psi_4 \end{pmatrix} = \begin{pmatrix} \cos\frac{\gamma}{2} & \sin\frac{\gamma}{2} \\ \sin\frac{\gamma}{2} & -\cos\frac{\gamma}{2} \end{pmatrix} \begin{pmatrix} b \\ d \end{pmatrix} = \begin{pmatrix} \cos\frac{\gamma}{2}b + \sin\frac{\gamma}{2}d \\ \sin\frac{\gamma}{2}b - \cos\frac{\gamma}{2}d \end{pmatrix} \tag{18}$$

This is the analogous transformation for inputs b and d by the beam splitter with parameter γ.

The outputs of the second stage, with parameter β, are:

$$\begin{pmatrix} \psi_{\text{out1}} \\ \psi_{\text{out2}} \end{pmatrix} = \begin{pmatrix} \cos\frac{\beta}{2} & \sin\frac{\beta}{2} \\ \sin\frac{\beta}{2} & -\cos\frac{\beta}{2} \end{pmatrix} \begin{pmatrix} \cos\frac{\alpha}{2}a + \sin\frac{\alpha}{2}c \\ \cos\frac{\gamma}{2}b + \sin\frac{\gamma}{2}d \end{pmatrix} \tag{19}$$

Here, the second stage beam splitter with parameter β acts on the outputs from the first stage.

Thus, the explicit expressions for ψ_{out1} and ψ_{out2} are

$$\begin{cases} \psi_{\text{out1}} = \cos\frac{\beta}{2}\cos\frac{\alpha}{2}a + \cos\frac{\beta}{2}\sin\frac{\alpha}{2}c + \sin\frac{\beta}{2}\cos\frac{\gamma}{2}b + \sin\frac{\beta}{2}\sin\frac{\gamma}{2}d, \\ \psi_{\text{out2}} = \sin\frac{\beta}{2}\cos\frac{\alpha}{2}a + \sin\frac{\beta}{2}\sin\frac{\alpha}{2}c - \cos\frac{\beta}{2}\cos\frac{\gamma}{2}b - \cos\frac{\beta}{2}\sin\frac{\gamma}{2}d. \end{cases} \tag{20}$$

These formulas give the output amplitudes after the second stage beam splitter with parameter β.

The other outputs at the second stage, with parameter κ, are given by:

$$\begin{pmatrix} \psi_{\text{out3}} \\ \psi_{\text{out4}} \end{pmatrix} = \begin{pmatrix} \cos\frac{\kappa}{2} & \sin\frac{\kappa}{2} \\ \sin\frac{\kappa}{2} & -\cos\frac{\kappa}{2} \end{pmatrix} \begin{pmatrix} \sin\frac{\alpha}{2}a - \cos\frac{\alpha}{2}c \\ e^{\frac{i\pi}{2}}\left(\sin\frac{\gamma}{2}b - \cos\frac{\gamma}{2}d\right) \end{pmatrix} \tag{21}$$

The second output pair from the second stage involves a phase factor $e^{i\pi/2}$ and is transformed by the beam splitter with parameter κ.

Hence,

$$\begin{cases} \psi_{\text{out3}} = \cos\frac{\kappa}{2}\sin\frac{\alpha}{2}a - \cos\frac{\kappa}{2}\cos\frac{\alpha}{2}c + e^{i\pi/2}\sin\frac{\kappa}{2}\sin\frac{\gamma}{2}b - e^{i\pi/2}\sin\frac{\kappa}{2}\cos\frac{\gamma}{2}d, \\ \psi_{\text{out4}} = \sin\frac{\kappa}{2}\sin\frac{\alpha}{2}a - \sin\frac{\kappa}{2}\cos\frac{\alpha}{2}c - e^{i\pi/2}\cos\frac{\kappa}{2}\sin\frac{\gamma}{2}b + e^{i\pi/2}\cos\frac{\kappa}{2}\cos\frac{\gamma}{2}d. \end{cases} \tag{22}$$

Explicit expressions for the output amplitudes ψ_{out3} and ψ_{out4}.

Special case:

If

$$\begin{pmatrix} a \\ b \end{pmatrix} = \begin{pmatrix} 1 \\ 0 \end{pmatrix}, \quad \begin{pmatrix} c \\ d \end{pmatrix} = \begin{pmatrix} 0 \\ 0 \end{pmatrix}, \tag{23}$$

This corresponds to the photon entering only the input mode a, with no photons in the other modes.

then

$$\psi_1 = \cos\frac{\alpha}{2}, \quad \psi_2 = \sin\frac{\alpha}{2}, \tag{24}$$

with corresponding probabilities

$$P_1 = |\psi_1|^2 = \cos^2\frac{\alpha}{2}, \quad P_2 = |\psi_2|^2 = \sin^2\frac{\alpha}{2}. \tag{25}$$

The output probabilities at the first beam splitter depend on the parameter α.

For $\alpha = \frac{\pi}{2}$, the probabilities become

$$P_1 = P_2 = \frac{1}{2}. \tag{26}$$

At this value, the beam splitter acts as a 50:50 splitter.

Since $\psi_3 = \psi_4 = 0$, the outputs reduce to

$$\begin{aligned} \psi_{\text{out1}} &= \cos\frac{\beta}{2}\cos\frac{\alpha}{2}, \quad \psi_{\text{out2}} = \sin\frac{\beta}{2}\cos\frac{\alpha}{2}, \\ \psi_{\text{out3}} &= \cos\frac{\kappa}{2}\sin\frac{\alpha}{2}, \quad \psi_{\text{out4}} = \sin\frac{\kappa}{2}\sin\frac{\alpha}{2}. \end{aligned} \tag{27}$$

The outputs depend on the parameters α, β, κ in this special input scenario.

The probabilities of detecting the photon at each output port are

$$\begin{aligned} P_{\text{out1}} &= \cos^2\frac{\beta}{2}\cos^2\frac{\alpha}{2}, \quad P_{\text{out2}} = \sin^2\frac{\beta}{2}\cos^2\frac{\alpha}{2}, \\ P_{\text{out3}} &= \cos^2\frac{\kappa}{2}\sin^2\frac{\alpha}{2}, \quad P_{\text{out4}} = \sin^2\frac{\kappa}{2}\sin^2\frac{\alpha}{2}. \end{aligned} \tag{28}$$

These represent the probabilities to detect the photon at each output port after the full circuit.

If $\alpha = \beta = \gamma = \kappa$, then

$$P_{\text{out1}} + P_{\text{out2}} + P_{\text{out3}} + P_{\text{out4}} = \cos^4\frac{\alpha}{2} + 2\cos^2\frac{\alpha}{2}\sin^2\frac{\alpha}{2} + \sin^4\frac{\alpha}{2} = 1. \tag{29}$$

This confirms the total probability is conserved and equals 1, as expected physically. Fig. 5 shows the probability distribution as a function of α.

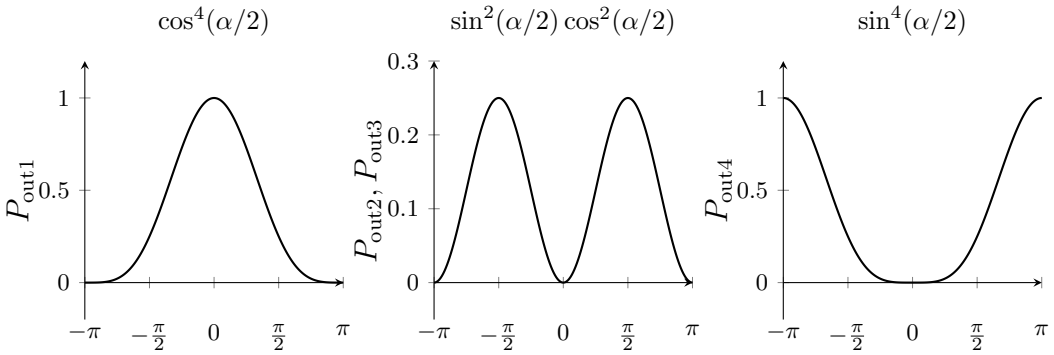


Fig. 5: Probability of detecting a photon at each output for a 2-qubit system, with initial conditions $a = 1$, $b = c = d = 0$, as α varies from $-\pi$ to π.

4.1.2 Effects of Imperfections and Error Analysis

In realistic experimental setups, ideal parameter values $\alpha, \beta, \gamma, \kappa$ are difficult to achieve due to manufacturing tolerances, imperfect alignment, optical losses, and environmental noise. These imperfections cause deviations from ideal splitting ratios and introduce

phase errors, which degrade the fidelity of the quantum Fourier transform implementation. For instance, deviations such as $\delta\alpha$ from the ideal value $\alpha_0 = \frac{\pi}{2}$ alter the output probabilities approximately as follows:

$$P_{\text{out1}} = \cos^2\frac{\beta}{2}\cos^2\left(\frac{\alpha_0}{2} + \frac{\delta\alpha}{2}\right), \tag{30}$$

$$P_{\text{out3}} = \cos^2\frac{\kappa}{2}\sin^2\left(\frac{\alpha_0}{2} + \frac{\delta\alpha}{2}\right). \tag{31}$$

Such deviations produce non-uniform photon distributions at the output ports, decreasing the operation's accuracy and fidelity. Figure 5 illustrates the probability distribution of photon detection at each output as a function of the parameter α. The plots show $\cos^4(\alpha/2)$, $\sin^2(\alpha/2)\cos^2(\alpha/2)$, and $\sin^4(\alpha/2)$ corresponding to different output ports. This visualization helps to understand how variations in α affect output probabilities. Furthermore, the relationship between parameter deviations and output probability changes can be used to estimate the magnitude of imperfections in optical components. For small deviations $\delta\alpha$, the output probability P_{out1} can be expanded as:

$$P_{\text{out1}}(\alpha) \approx P_{\text{out1}}(\alpha_0) + \left.\frac{\partial P_{\text{out1}}}{\partial\alpha}\right|_{\alpha_0}\delta\alpha, \tag{32}$$

where the partial derivative is

$$\frac{\partial P_{\text{out1}}}{\partial\alpha} = -\cos^2\frac{\beta}{2}\sin\alpha. \tag{33}$$

Therefore, the deviation $\delta\alpha$ can be estimated from the output probability by comparing it with its ideal theoretical value

$$\delta\alpha \approx \frac{P_{\text{out1}} - P_{\text{out1}}^{\text{ideal}}}{\left.\frac{\partial P_{\text{out1}}}{\partial\alpha}\right|_{\alpha_0}}. \tag{34}$$

For example, suppose the ideal parameter value is $\alpha_0 = \frac{\pi}{2}$ and $\beta = \kappa = \frac{\pi}{2}$. Then, from Eq. (30), the ideal output probability is

$$P_{\text{out1}}^{\text{ideal}} = \cos^2\frac{\beta}{2}\cos^2\frac{\alpha_0}{2} = \cos^2\frac{\pi}{4}\cos^2\frac{\pi}{4} = \left(\frac{\sqrt{2}}{2}\right)^2 \times \left(\frac{\sqrt{2}}{2}\right)^2 = \frac{1}{4}. \tag{35}$$

For a numerical illustration, assume that the output probability is $P_{\text{out1}} = 0.30$. From Eq. (33), the partial derivative at $\alpha_0 = \frac{\pi}{2}$ is

$$\left.\frac{\partial P_{\text{out1}}}{\partial\alpha}\right|_{\alpha_0} = -\cos^2\frac{\beta}{2}\sin\alpha_0 = -\cos^2\frac{\pi}{4}\sin\frac{\pi}{2} = -\frac{1}{2}\times 1 = -\frac{1}{2}. \tag{36}$$

Using Eq. (34), the estimated deviation $\delta\alpha$ is

$$\delta\alpha \approx \frac{0.30 - 0.25}{-\frac{1}{2}} = \frac{0.05}{-0.5} = -0.1, \tag{37}$$

which means the actual parameter α deviates by about -0.1 radians (approximately $-5.7°$) from the ideal value $\frac{\pi}{2}$. This numerical example shows how deviations in the output probability can be used to quantify imperfections in optical components. Therefore, by comparing the calculated output probabilities with their ideal theoretical values and applying first-order expansions, the corresponding parameter deviations can be estimated. This theoretical error analysis provides a framework for diagnosing and quantifying the effects of imperfections in optical components. Therefore, by comparing measured output probabilities with ideal theoretical values and applying first-order expansions, one can effectively estimate the parameter deviations due to imperfections. This error analysis is essential for diagnosing and correcting imperfections, thereby improving the fidelity of quantum optical experiments. If we assume that the parameters α and β vary simultaneously and equally, i.e., $\beta = \alpha = \alpha_0 + \delta\alpha$, then the output probability P_{out1} becomes

$$P_{\text{out1}} = \cos^2\frac{\beta}{2}\cos^2\frac{\alpha}{2} = \cos^4\frac{\alpha}{2}. \tag{38}$$

By performing a first-order Taylor expansion around the ideal value $\alpha_0 = \frac{\pi}{2}$, we have

$$P_{\text{out1}}(\alpha) \approx P_{\text{out1}}(\alpha_0) + \left.\frac{dP_{\text{out1}}}{d\alpha}\right|_{\alpha_0}\delta\alpha, \tag{39}$$

where the derivative is

$$\frac{dP_{\text{out1}}}{d\alpha} = -2\cos^3\frac{\alpha}{2}\sin\frac{\alpha}{2}. \tag{40}$$

Evaluating at $\alpha_0 = \frac{\pi}{2}$ gives

$$\left.\frac{dP_{\text{out1}}}{d\alpha}\right|_{\alpha_0} = -2\left(\frac{\sqrt{2}}{2}\right)^3\left(\frac{\sqrt{2}}{2}\right) = -2\times\frac{\sqrt{2}^4}{2^4} = -\frac{1}{2}. \tag{41}$$

Therefore, the deviation $\delta\alpha$ can be estimated from the difference between the measured and ideal output probabilities as

$$\delta\alpha \approx \frac{P_{\text{out1}} - P_{\text{out1}}^{\text{ideal}}}{\left.\frac{dP_{\text{out1}}}{d\alpha}\right|_{\alpha_0}} = -2\left(P_{\text{out1}}^{\text{real}} - P_{\text{out1}}^{\text{ideal}}\right). \tag{42}$$

Assuming α and β vary together such that $\beta = \alpha = \alpha_0 + \delta\alpha$, with the ideal value $\alpha_0 = \frac{\pi}{2}$, the ideal output probability from Eq. (38) becomes

$$P_{\text{out1}}^{\text{ideal}} = \cos^4\frac{\alpha_0}{2} = \left(\cos\frac{\pi}{4}\right)^4 = \left(\frac{\sqrt{2}}{2}\right)^4 = \frac{1}{4}. \tag{43}$$

For the same numerical example, if the output probability is $P_{\text{out1}} = 0.30$, then using the derivative in Eq. (41), we estimate the deviation $\delta\alpha$ as

$$\delta\alpha \approx \frac{0.30 - 0.25}{-\frac{1}{2}} = -0.1, \tag{44}$$

which corresponds to approximately $-5.7°$. This shows that when α and β deviate equally, the estimation of $\delta\alpha$ from the measured output probability is straightforward and similar in form to the single-parameter case. Such analysis can be extended to other output probabilities and parameters, enabling precise calibration of optical components in quantum circuits.

Figure 6 shows the exact function $P_{\text{out1}}(\alpha) = \cos^4(\alpha/2)$ (solid line) along with its first-order Taylor approximation around $\alpha_0 = \frac{\pi}{2}$ (dashed line). The close match near α_0 demonstrates the validity of the linear approximation for small deviations.

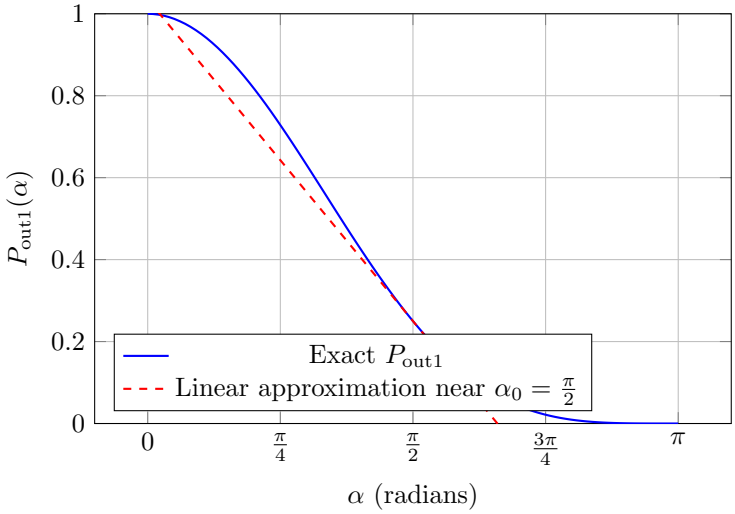


Fig. 6: Exact output probability $P_{\text{out1}}(\alpha) = \cos^4(\alpha/2)$ and its linear approximation near $\alpha_0 = \frac{\pi}{2}$.

This theoretical error analysis allows parameter deviations to be estimated from output probabilities using first-order Taylor expansions. The approach provides a practical theoretical framework for identifying and quantifying imperfections in optical components and for assessing their impact on the accuracy and fidelity of quantum Fourier transform implementations. These results can be useful for the future calibration and optimization of experimental optical quantum circuits. In the next section, we will discuss the system representation as a matrix. Then, we will analyze the system for three qubits, and finally, we will extend the problem to an arbitrary number of qubits.

4.1.3 System Representation as a Matrix

An alternative viewpoint on the entire system treats all optical elements involved in the QFT as a single unitary operator. To realize this, each stage may be analyzed individually, as detailed in **Appendix B**, or by employing the QFT method described in **Section 2** and Equation (13), considering the beam splitters as imperfect.

$$\begin{pmatrix} \psi_{out1} \\ \psi_{out2} \\ \psi_{out3} \\ \psi_{out4} \end{pmatrix} = \begin{pmatrix} \cos\frac{\beta}{2} & \sin\frac{\beta}{2} & 0 & 0 \\ \sin\frac{\beta}{2} & -\cos\frac{\beta}{2} & 0 & 0 \\ 0 & 0 & \cos\frac{\kappa}{2} & e^{i\pi/2}\sin\frac{\kappa}{2} \\ 0 & 0 & \sin\frac{\kappa}{2} & e^{3i\pi/2}\cos\frac{\kappa}{2} \end{pmatrix} \begin{pmatrix} \cos\frac{\alpha}{2} & 0 & \sin\frac{\alpha}{2} & 0 \\ 0 & \cos\frac{\gamma}{2} & 0 & \sin\frac{\gamma}{2} \\ \sin\frac{\alpha}{2} & 0 & -\cos\frac{\alpha}{2} & 0 \\ 0 & \sin\frac{\gamma}{2} & 0 & -\cos\frac{\gamma}{2} \end{pmatrix} \begin{pmatrix} a \\ b \\ c \\ d \end{pmatrix} \tag{45}$$

After multiplying the two matrices, the resulting expression is:

$$\begin{pmatrix} \psi_{out1} \\ \psi_{out2} \\ \psi_{out3} \\ \psi_{out4} \end{pmatrix} = \begin{pmatrix} \cos\frac{\alpha}{2}\cos\frac{\beta}{2} & \sin\frac{\beta}{2}\cos\frac{\gamma}{2} & \cos\frac{\beta}{2}\sin\frac{\alpha}{2} & \sin\frac{\beta}{2}\sin\frac{\gamma}{2} \\ \sin\frac{\beta}{2}\cos\frac{\alpha}{2} & -\cos\frac{\beta}{2}\cos\frac{\gamma}{2} & \sin\frac{\alpha}{2}\sin\frac{\beta}{2} & -\cos\frac{\beta}{2}\sin\frac{\gamma}{2} \\ \cos\frac{\kappa}{2}\sin\frac{\alpha}{2} & e^{i\pi/2}\sin\frac{\gamma}{2}\sin\frac{\kappa}{2} & -\cos\frac{\kappa}{2}\cos\frac{\alpha}{2} & -e^{i\pi/2}\sin\frac{\kappa}{2}\cos\frac{\gamma}{2} \\ \sin\frac{\kappa}{2}\sin\frac{\alpha}{2} & -e^{i\pi/2}\cos\frac{\kappa}{2}\sin\frac{\gamma}{2} & -\sin\frac{\kappa}{2}\sin\frac{\alpha}{2} & e^{i\pi/2}\cos\frac{\gamma}{2}\cos\frac{\kappa}{2} \end{pmatrix} \begin{pmatrix} a \\ b \\ c \\ d \end{pmatrix} \tag{46}$$

The output states are explicitly given by:

$$\begin{cases} \psi_{out1} = \cos\frac{\alpha}{2}\cos\frac{\beta}{2}\,a + \sin\frac{\beta}{2}\cos\frac{\gamma}{2}\,b + \cos\frac{\beta}{2}\sin\frac{\alpha}{2}\,c + \sin\frac{\beta}{2}\sin\frac{\gamma}{2}\,d \\ \psi_{out2} = \sin\frac{\beta}{2}\cos\frac{\alpha}{2}\,a - \cos\frac{\beta}{2}\cos\frac{\gamma}{2}\,b + \sin\frac{\alpha}{2}\sin\frac{\beta}{2}\,c - \cos\frac{\beta}{2}\sin\frac{\gamma}{2}\,d \\ \psi_{out3} = \cos\frac{\kappa}{2}\sin\frac{\alpha}{2}\,a + e^{i\pi/2}\sin\frac{\gamma}{2}\sin\frac{\kappa}{2}\,b - \cos\frac{\kappa}{2}\cos\frac{\alpha}{2}\,c - e^{i\pi/2}\sin\frac{\kappa}{2}\cos\frac{\gamma}{2}\,d \\ \psi_{out4} = \sin\frac{\kappa}{2}\sin\frac{\alpha}{2}\,a - e^{i\pi/2}\cos\frac{\kappa}{2}\sin\frac{\gamma}{2}\,b - \sin\frac{\kappa}{2}\sin\frac{\alpha}{2}\,c + e^{i\pi/2}\cos\frac{\gamma}{2}\cos\frac{\kappa}{2}\,d \end{cases}$$

From this point, we define the parameters as $\alpha = \theta_{00}$, $\gamma = \theta_{10}$, $\beta = \theta_{01}$, and $\kappa = \theta_{11}$, as illustrated in Fig. 4 within the beam splitters. These definitions simplify calculations and facilitate extension to larger systems. The derivation is detailed in **Appendix B**.

$$\begin{aligned} \psi_{out1} &= \cos\frac{\theta_{00}}{2}\cos\frac{\theta_{01}}{2}a + \sin\frac{\theta_{01}}{2}\cos\frac{\theta_{10}}{2}b + \sin\frac{\theta_{00}}{2}\cos\frac{\theta_{01}}{2}c + \sin\frac{\theta_{01}}{2}\sin\frac{\theta_{10}}{2}d \\ \psi_{out2} &= \cos\frac{\theta_{00}}{2}\sin\frac{\theta_{01}}{2}a - \cos\frac{\theta_{01}}{2}\cos\frac{\theta_{10}}{2}b + \sin\frac{\theta_{00}}{2}\sin\frac{\theta_{01}}{2}c - \cos\frac{\theta_{01}}{2}\sin\frac{\theta_{10}}{2}d \\ \psi_{out3} &= \cos\frac{\theta_{00}}{2}\cos\frac{\theta_{11}}{2}a + e^{i\pi/2}\sin\frac{\theta_{10}}{2}\sin\frac{\theta_{11}}{2}b - \cos\frac{\theta_{00}}{2}\cos\frac{\theta_{11}}{2}c - e^{i\pi/2}\cos\frac{\theta_{10}}{2}\sin\frac{\theta_{11}}{2}d \\ \psi_{out4} &= \cos\frac{\theta_{00}}{2}\sin\frac{\theta_{11}}{2}a + e^{3i\pi/2}\sin\frac{\theta_{10}}{2}\cos\frac{\theta_{11}}{2}b - \cos\frac{\theta_{00}}{2}\sin\frac{\theta_{11}}{2}c + e^{3i\pi/2}\cos\frac{\theta_{10}}{2}\cos\frac{\theta_{11}}{2}d \end{aligned} \tag{47}$$

As demonstrated in **Appendix B**, the output values are computed in two steps: first by calculating the intermediate states ψ_1 to ψ_4, then by determining the output states $\psi_{\text{out},1}$ to $\psi_{\text{out},4}$.

To maintain a structured and consistent notation, similar to Equation (14), the inputs are denoted by $|x_0\rangle$. For example, $|x_0(0,0)\rangle$ corresponds to a, $|x_0(0,1)\rangle$ to b, $|x_0(1,0)\rangle$ to c, and $|x_0(1,1)\rangle$ to d, representing the initial input states.

At the intermediate stage, the states $|x_1(0,0)\rangle$, $|x_1(0,1)\rangle$, $|x_1(1,0)\rangle$, and $|x_1(1,1)\rangle$ correspond to ψ_1, ψ_2, ψ_3, and ψ_4, respectively. Similarly, the output states $|x_2(0,0)\rangle$, $|x_2(0,1)\rangle$, $|x_2(1,0)\rangle$, and $|x_2(1,1)\rangle$ correspond to $\psi_{\text{out1}}, \psi_{\text{out2}}, \psi_{\text{out3}}$, and ψ_{out4}, respectively.

In the two-qubit case, this notation enables a clear and structured representation of the OQFT circuit, allowing for a generalized formula that captures the transformations from input states $|x_0(i,j)\rangle$, through intermediate states $|x_1(i,j)\rangle$, to the final output states $|x_2(i,j)\rangle$.

The extended form of the equation can be written as:

$$
\begin{aligned}
|x_1(n_0,k_0)\rangle &= \sum_{k_1=0}^{1} W^{2n_0k_1} \cos^{1-n_0}\left(\frac{\theta_{k_0 0}}{2} - k_1\frac{\pi}{2}\right) \sin^{n_0}\left(\frac{\theta_{k_0 0}}{2} + k_1\frac{\pi}{2}\right) |x_0(k_1,k_0)\rangle \\
|x_2(n_0,n_1)\rangle &= \sum_{k_0=0}^{1} W^{(2n_1+n_0)k_0} \cos^{1-n_1}\left(\frac{\theta_{n_0 1}}{2} - k_0\frac{\pi}{2}\right) \sin^{n_1}\left(\frac{\theta_{n_0 1}}{2} + k_0\frac{\pi}{2}\right) |x_1(n_0,k_0)\rangle \\
|\boldsymbol{X}(n_1,n_0)\rangle &= |\boldsymbol{x}_2(n_0,n_1)\rangle
\end{aligned}
\tag{48}
$$

4.2 Three-qubit system

In the previous subsection, a two-qubit system was investigated from two perspectives: first, by considering each beam splitter individually and deriving the equation for the general structure, and second, by treating the entire system as a unitary matrix. Both approaches yielded the same result. In this subsection, we extend the analysis to a three-qubit system and derive the unitary matrix of the whole system.

$$
\begin{pmatrix}
|x_2(0,0,0)\rangle \\ |x_2(0,0,1)\rangle \\ |x_2(0,1,0)\rangle \\ |x_2(0,1,1)\rangle \\ |x_2(1,0,0)\rangle \\ |x_2(1,0,1)\rangle \\ |x_2(1,1,0)\rangle \\ |x_2(1,1,1)\rangle
\end{pmatrix}
= M_3 \times M_2 \times M_1
\begin{pmatrix}
|x_0(0,0,0)\rangle \\ |x_0(0,0,1)\rangle \\ |x_0(0,1,0)\rangle \\ |x_0(0,1,1)\rangle \\ |x_0(1,0,0)\rangle \\ |x_0(1,0,1)\rangle \\ |x_0(1,1,0)\rangle \\ |x_0(1,1,1)\rangle
\end{pmatrix}
\tag{49}
$$

Where the matrices M_1, M_2, M_3 are given by:

$$M_1 = \begin{bmatrix} W^0 & 0 & 0 & 0 & W^0 & 0 & 0 & 0 \\ 0 & W^0 & 0 & 0 & 0 & W^0 & 0 & 0 \\ 0 & 0 & W^0 & 0 & 0 & 0 & W^0 & 0 \\ 0 & 0 & 0 & W^0 & 0 & 0 & 0 & W^0 \\ W^0 & 0 & 0 & 0 & W^4 & 0 & 0 & 0 \\ 0 & W^0 & 0 & 0 & 0 & W^4 & 0 & 0 \\ 0 & 0 & W^0 & 0 & 0 & 0 & W^4 & 0 \\ 0 & 0 & 0 & W^0 & 0 & 0 & 0 & W^4 \end{bmatrix} \quad M_2 = \begin{bmatrix} W^0 & 0 & W^0 & 0 & 0 & 0 & 0 & 0 \\ 0 & W^0 & 0 & W^0 & 0 & 0 & 0 & 0 \\ W^0 & 0 & W^4 & 0 & 0 & 0 & 0 & 0 \\ 0 & W^0 & 0 & W^4 & 0 & 0 & 0 & 0 \\ 0 & 0 & 0 & 0 & W^0 & 0 & W^2 & 0 \\ 0 & 0 & 0 & 0 & 0 & W^0 & 0 & W^2 \\ 0 & 0 & 0 & 0 & W^0 & 0 & W^6 & 0 \\ 0 & 0 & 0 & 0 & 0 & W^0 & 0 & W^6 \end{bmatrix}$$

$$M_3 = \begin{bmatrix} W^0 & W^0 & 0 & 0 & 0 & 0 & 0 & 0 \\ W^0 & W^4 & 0 & 0 & 0 & 0 & 0 & 0 \\ 0 & 0 & W^0 & W^2 & 0 & 0 & 0 & 0 \\ 0 & 0 & W^0 & W^6 & 0 & 0 & 0 & 0 \\ 0 & 0 & 0 & 0 & W^0 & W^1 & 0 & 0 \\ 0 & 0 & 0 & 0 & W^0 & W^5 & 0 & 0 \\ 0 & 0 & 0 & 0 & 0 & 0 & W^0 & W^3 \\ 0 & 0 & 0 & 0 & 0 & 0 & W^0 & W^7 \end{bmatrix}$$

According to the calculation in **Appendix C**, we consider the case of three qubits, for which the quantum Fourier transform requires three stages. As in the previous section, the input values are denoted by $|x_0\rangle$, the outputs of the first stage by $|x_1\rangle$, and the final outputs by $|x_2\rangle$. Since we are dealing with three qubits, each stage involves eight possible input combinations, ranging from $(0,0,0)$ to $(1,1,1)$. Therefore, the expanded form of the relation can be written as follows: at each stage, the signal passes through one beam splitter. Given that there are three qubits, each photon passes through three beam splitters in total.

$$\begin{aligned} |x_1(n_0,k_1,k_0)\rangle = &\sum_{k_2=0}^{1} W^{4n_0k_2} \cos^{1-n_0}\left(\frac{\theta_{(2k_1+k_0)0}}{2} - k_2\frac{\pi}{2}\right) \\ &\times \sin^{n_0}\left(\frac{\theta_{(2k_1+k_0)0}}{2} + k_2\frac{\pi}{2}\right)|x_0(k_2,k_1,k_0)\rangle \end{aligned} \tag{50}$$

$$\begin{aligned} |x_2(n_0,n_1,k_0)\rangle = &\sum_{k_1=0}^{1} W^{(2n_1+n_0)(2k_1)} \cos^{1-n_1}\left(\frac{\theta_{(2n_0+k_0)1}}{2} - k_1\frac{\pi}{2}\right) \\ &\times \sin^{n_1}\left(\frac{\theta_{(2n_0+k_0)1}}{2} + k_1\frac{\pi}{2}\right)|x_1(n_0,k_1,k_0)\rangle \end{aligned}$$

$$\begin{aligned} |x_3(n_0,n_1,n_2)\rangle = &\sum_{k_0=0}^{1} W^{(4n_2+2n_1+n_0)k_0} \cos^{1-n_2}\left(\frac{\theta_{(2n_0+n_1)2}}{2} - k_0\frac{\pi}{2}\right) \\ &\times \sin^{n_2}\left(\frac{\theta_{(2n_0+n_1)2}}{2} + k_0\frac{\pi}{2}\right)|x_2(n_0,n_1,k_0)\rangle \end{aligned}$$

$$|\boldsymbol{X}(\boldsymbol{n_2},\boldsymbol{n_1},\boldsymbol{n_0})\rangle = |\boldsymbol{x}_3(\boldsymbol{n_0},\boldsymbol{n_1},\boldsymbol{n_2})\rangle$$

4.3 γ-qubit system

For the general case of a system composed of γ qubits, the quantum transformation can be described in a systematic and recursive manner involving γ successive stages. The input states are denoted as:

$$|x_0(i_0, i_1, \ldots, i_{\gamma-1})\rangle\,,$$

where each $i_k \in \{0, 1\}$ for $k = 0, 1, \ldots, \gamma - 1$, representing all possible binary combinations of the qubit basis states. For instance, in the two-qubit case, there are $2^2 = 4$ input states ranging from $|x_0(0, 0)\rangle$ to $|x_0(1, 1)\rangle$, and for three qubits, the number increases to $2^3 = 8$ input states, from $|x_0(0, 0, 0)\rangle$ to $|x_0(1, 1, 1)\rangle$.

These input states undergo transformations through γ consecutive stages, where each stage k applies specific unitary operations to the system, usually realized by beam splitters and phase shifters in an optical quantum computing setup. At stage k, the intermediate states are denoted by

$$|x_k(i_0, i_1, \ldots, i_{\gamma-1})\rangle\,,$$

which encode the partial transformations applied up to that stage. This hierarchical, stage-wise process continues until the final output states

$$|x_\gamma(i_0, i_1, \ldots, i_{\gamma-1})\rangle$$

are obtained, corresponding to the fully transformed outputs of the Optical Quantum Fourier Transform (OQFT), as schematically shown in Fig. 7.

The unitary operations at each stage are constructed from an arrangement of beam splitters and phase shifters, each represented by matrices m_{ij} where the indices i and j specify the position of the corresponding beam splitter within the optical circuit's matrix representation. This systematic indexing allows for a compact and scalable mathematical description of the entire OQFT circuit.

Moreover, the recursive structure and layered decomposition of the transformation make it possible to implement the OQFT efficiently for any number of qubits. This is crucial because the size of the Hilbert space grows exponentially with γ, and the described architecture ensures that the transformation remains manageable by breaking it down into a sequence of simpler, localized unitary operations.

In summary, the γ-qubit system's OQFT can be viewed as a composition of γ unitary layers, each corresponding to a stage of beam splitter arrays and phase adjustments, effectively generalizing the well-known quantum Fourier transform algorithm into an experimentally realizable optical network.

$$
\begin{aligned}
|x_1(n_0, k_{\gamma-2}, k_{\gamma-3}, ..., k_0)\rangle = &\sum_{k_{\gamma-1}=0}^{1} W^{4n_0 k_{\gamma-1}} \cos^{(1-n_0)}\left(\tfrac{\theta_{m_0 0}}{2} - k_{\gamma-1}\tfrac{\pi}{2}\right) \sin^{n_0}\left(\tfrac{\theta_{m_0 0}}{2} + k_{\gamma-1}\tfrac{\pi}{2}\right) \\
&\times |x_0(k_{\gamma-1}, k_{\gamma-2}, ..., k_0)\rangle \\
m_0 = &\, 2^{\gamma-2}k_{\gamma-2} + 2^{\gamma-3}k_{\gamma-3} + \cdots + 2^1 k_1 + 2^0 k_0 \\
|x_2(n_0, n_1, k_{\gamma-3}, ..., k_0)\rangle = &\sum_{k_{\gamma-2}=0}^{1} W^{(2n_1+n_0)(2k_{\gamma-2})} \cos^{(1-n_1)}\left(\tfrac{\theta_{m_1 1}}{2} - k_{\gamma-2}\tfrac{\pi}{2}\right) \sin^{n_1}\left(\tfrac{\theta_{m_1 1}}{2} + k_{\gamma-2}\tfrac{\pi}{2}\right) \\
&\times |x_1(n_0, k_{\gamma-2}, k_{\gamma-3}, ..., k_0)\rangle \\
m_1 = &\, 2^{\gamma-1}n_0 + 2^{\gamma-3}k_{\gamma-3} + 2^{\gamma-4}k_{\gamma-4} + \cdots + 2^1 k_1 + 2^0 k_0 \\
&\vdots \\
|x_\gamma(n_0, n_1, ..., n_{\gamma-1})\rangle = &\sum_{k_0=0}^{1} W^{(2^{\gamma-1}n_{\gamma-1} + 2^{\gamma-2}n_{\gamma-2} + \cdots + n_0)(k_0)} \cos^{(1-n_{\gamma-1})}\left(\tfrac{\theta_{m_{\gamma-1},\gamma-1}}{2} - k_0\tfrac{\pi}{2}\right) \\
&\times \sin^{n_{\gamma-1}}\left(\tfrac{\theta_{m_{\gamma-1},\gamma-1}}{2} + k_0\tfrac{\pi}{2}\right) |x_{\gamma-1}(n_0, n_1, ..., k_0)\rangle \\
m_{\gamma-1} = &\, 2^{\gamma-1}n_0 + 2^{\gamma-2}n_1 + 2^{\gamma-3}n_2 + \cdots + 2^1 n_{\gamma-2} \\
&|\boldsymbol{X}(\boldsymbol{n_{\gamma-1}}, \ldots, \boldsymbol{n_0})\rangle = |\boldsymbol{x}_\gamma(\boldsymbol{n_0}, \ldots, \boldsymbol{n_{\gamma-1}})\rangle
\end{aligned}
\tag{51}
$$

5 Phase Error in Path Difference

So far, the effect of imperfections in beam splitters has been investigated; however, phase shifts caused by differences in optical path lengths, as introduced in **Section 2**, represent another significant source of error in the Optical Quantum Fourier Transform (OQFT).

Consider a beam splitter with two input ports labeled 1 and 2. Let L_1 and L_2 denote the optical path lengths that photons travel to reach these input ports. The phase difference accumulated by photons traveling these paths can be expressed by the diagonal matrix:

$$
L(L_1, L_2) = \begin{pmatrix} e^{\frac{2\pi i L_1}{\lambda}} & 0 \\ 0 & e^{\frac{2\pi i L_2}{\lambda}} \end{pmatrix} \tag{52}
$$

where λ is the wavelength of the photons.

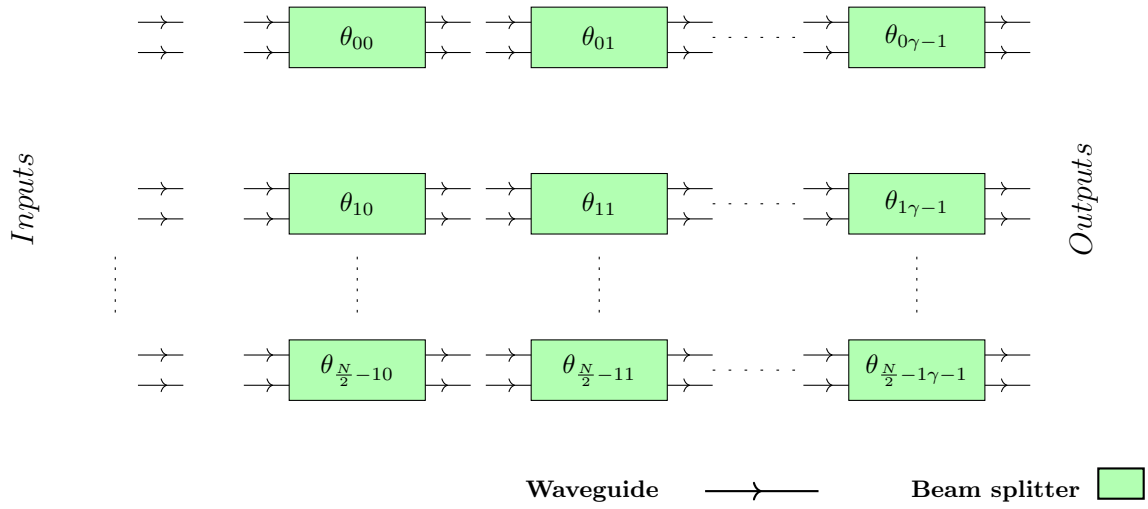


Fig. 7: An optical implementation of a γ-qubit QFT circuit. The inputs, corresponding to quantum modes or photons, enter from the left and propagate through the circuit to the outputs on the right. Each green rectangle represents a beam splitter (BS) characterized by a splitting angle θ. The horizontal arrows denote optical waveguides carrying quantum information, while the multiple BS stages together implement the unitary transformation associated with QFT. The structure follows a Cooley–Tukey-style decomposition, where each column corresponds to a layer of beam splitter operations acting on selected mode pairs. Dashed vertical lines indicate the column boundaries (stages), and dashed horizontal lines represent symmetry or pairing in mode interaction.

When extending the system to multiple inputs, for instance in a four-input case (corresponding to two qubits), the combined transformation including phase shifts and beam splitter rotations can be written as:

$$\begin{pmatrix}\psi_1\\ \psi_2\\ \psi_3\\ \psi_4\end{pmatrix} = \underbrace{\begin{pmatrix}\cos\frac{\theta_{00}}{2} & 0 & \sin\frac{\theta_{00}}{2} & 0\\ 0 & \cos\frac{\theta_{10}}{2} & 0 & \sin\frac{\theta_{10}}{2}\\ \sin\frac{\theta_{00}}{2} & 0 & -\cos\frac{\theta_{00}}{2} & 0\\ 0 & \sin\frac{\theta_{10}}{2} & 0 & -\cos\frac{\theta_{10}}{2}\end{pmatrix}}_{U} \underbrace{\begin{pmatrix}e^{\frac{2\pi i L_{00}}{\lambda}} & 0 & 0 & 0\\ 0 & e^{\frac{2\pi i L_{10}}{\lambda}} & 0 & 0\\ 0 & 0 & e^{\frac{2\pi i L_{20}}{\lambda}} & 0\\ 0 & 0 & 0 & e^{\frac{2\pi i L_{30}}{\lambda}}\end{pmatrix}}_{D} \begin{pmatrix}a\\ b\\ c\\ d\end{pmatrix} \tag{53}$$

Here, U represents the unitary transformation imposed by the beam splitters and phase shifters, and D accounts for the phase shifts due to the different path lengths L_{ij}.

The above form can be generalized recursively to multi-stage transformations. For instance, at the first stage:

$$|x_1(n_0,k_0)\rangle = \sum_{k_1=0}^{1} W^{2n_0k_1}\ \cos^{(1-n_0)}\left(\frac{\theta_{k_0 0}}{2} - k_1\frac{\pi}{2}\right)\sin^{n_0}\left(\frac{\theta_{k_0 0}}{2} + k_1\frac{\pi}{2}\right) \times e^{\frac{2\pi i L_{(2k_1+k_0)0}}{\lambda}}\,|x_0(k_1,k_0)\rangle \tag{54}$$

and for the second stage:

$$|x_2(n_0,n_1)\rangle = \sum_{k_0=0}^{1} W^{(2n_1+n_0)k_0}\ \cos^{(1-n_1)}\left(\frac{\theta_{n_0 1}}{2} - k_0\frac{\pi}{2}\right)\sin^{n_1}\left(\frac{\theta_{n_0 1}}{2} + k_0\frac{\pi}{2}\right) \times e^{\frac{2\pi i L_{(2n_0+k_0)1}}{\lambda}}\,|x_1(n_0,k_0)\rangle \tag{55}$$

For a general γ-stage OQFT circuit with $N = 2^\gamma$ inputs, the recursive relation for the k-th stage can be expressed as:

$$\begin{aligned}
|x_1(n_0,k_{\gamma-2},k_{\gamma-3},\ldots,k_0)\rangle = &\sum_{k_{\gamma-1}=0}^{1} W^{4n_0k_{\gamma-1}}\cos^{(1-n_0)}\left(\tfrac{\theta_{m_0 0}}{2} - k_{\gamma-1}\tfrac{\pi}{2}\right)\\
&\times\sin^{n_0}\left(\tfrac{\theta_{m_0 0}}{2} + k_{\gamma-1}\tfrac{\pi}{2}\right)e^{\frac{2\pi i L_{h_0 0}}{\lambda}}|x_0(k_{\gamma-1},k_{\gamma-2},\ldots,k_0)\rangle\\
|x_2(n_0,n_1,k_{\gamma-3},\ldots,k_0)\rangle = &\sum_{k_{\gamma-2}=0}^{1} W^{(2n_1+n_0)(2k_{\gamma-2})}\cos^{(1-n_1)}\left(\tfrac{\theta_{m_1 1}}{2} - k_{\gamma-2}\tfrac{\pi}{2}\right)\\
&\times\sin^{n_1}\left(\tfrac{\theta_{m_1 1}}{2} + k_{\gamma-2}\tfrac{\pi}{2}\right)e^{\frac{2\pi i L_{h_1 1}}{\lambda}}|x_1(n_0,k_{\gamma-2},k_{\gamma-3},\ldots,k_0)\rangle\\
&\vdots\\
|x_\gamma(n_0,n_1,\ldots,n_{\gamma-1})\rangle = &\sum_{k_0=0}^{1} W^{(2^{\gamma-1}n_{\gamma-1}+\cdots+n_0)k_0}\cos^{(1-n_{\gamma-1})}\left(\tfrac{\theta_{(m_{\gamma-1})(\gamma-1)}}{2} - k_0\tfrac{\pi}{2}\right)\\
&\times\sin^{n_{\gamma-1}}\left(\tfrac{\theta_{(m_{\gamma-1})(\gamma-1)}}{2} + k_0\tfrac{\pi}{2}\right)e^{\frac{2\pi i L_{h_{\gamma-1}(\gamma-1)}}{\lambda}}|x_{\gamma-1}(n_0,n_1,\ldots,k_0)\rangle\\
&|\boldsymbol{X(n_{\gamma-1},\ldots,n_0)}\rangle = |\boldsymbol{x_\gamma(n_0,n_1,\ldots,n_{\gamma-1})}\rangle
\end{aligned} \tag{56}$$

Finally, the fully transformed output state after γ stages is:

$$|\boldsymbol{X(n_{\gamma-1},\ldots,n_0)}\rangle = |\boldsymbol{x_\gamma(n_0,n_1,\ldots,n_{\gamma-1})}\rangle \tag{57}$$

Here, $W = e^{2\pi i/N}$ is the N-th root of unity appearing in the quantum Fourier transform, $\theta_{m_{ij}}$ are the parameters related to beam splitter reflectivities, and $L_{h_{ij}}$ represent the path length-dependent phase shifts for each stage and mode. This formalism captures how phase errors induced by optical path differences propagate through the multi-stage OQFT circuit, modifying the interference pattern and thereby affecting the accuracy of the quantum transform. Careful design and compensation of these phases are essential for high-fidelity OQFT implementations.

6 conclusion and a summary

This paper presents a novel approach to implementing the QFT via linear optical setups, based on the Cooley–Tukey algorithm, while thoroughly investigating the influence of non-idealities in optical components.

The Cooley–Tukey method, known for its recursive decomposition of the DFT, allows breaking down a $2^\gamma \times 2^\gamma$ unitary operation into γ sequential layers, each containing $2^{\gamma-1}$ smaller unitary blocks. Such a hierarchical structure facilitates an efficient deployment of QFT circuits using fewer beam splitters (BS) and phase shifters (PS), enhancing scalability. Leveraging this recursive framework, the study performs a comprehensive error propagation analysis at each stage, focusing on how imperfections in optical elements accumulate and affect system performance.

The investigation covers specific cases of two- and three-qubit systems before generalizing to an arbitrary n-qubit architecture, culminating in a universal formula valid for any γ-qubit configuration. Moreover, the role of optical path length variations on phase deviations in the output is critically evaluated, addressing practical challenges in device fabrication and alignment.

The outcomes of this research hold significant importance for the advancement of quantum integrated photonics, where managing physical imperfections is pivotal for developing scalable and fault-tolerant quantum circuits. In comparison to earlier studies, our model offers a broader and more adaptable framework for error characterization in realistic optical components.

Additionally, the clear modularity provided by the Cooley–Tukey algorithm opens pathways for integrating dynamic error correction protocols, potentially leading to enhanced fidelity and robustness in photonic quantum information processing.

A Derivation of Eq. (11)

The matrix presented in equation (9) can be written as follows:

$$\begin{pmatrix} |X(0,0)\rangle \\ |X(1,0)\rangle \\ |X(0,1)\rangle \\ |X(1,1)\rangle \end{pmatrix} = \frac{1}{2} \begin{pmatrix} 1 & W^0 & 0 & 0 \\ 1 & W^2 & 0 & 0 \\ 0 & 0 & 1 & W^1 \\ 0 & 0 & 1 & W^3 \end{pmatrix} \begin{pmatrix} 1 & 0 & W^0 & 0 \\ 0 & 1 & 0 & W^0 \\ 1 & 0 & W^2 & 0 \\ 0 & 1 & 0 & W^2 \end{pmatrix} \begin{pmatrix} |x_0(0,0)\rangle \\ |x_0(0,1)\rangle \\ |x_0(1,0)\rangle \\ |x_0(1,1)\rangle \end{pmatrix} \tag{58}$$

The vector on the left side of Eq. (58) is denoted as $\overline{X(n)}$:

$$\overline{X(n)} = \begin{pmatrix} |X(0,0)\rangle \\ |X(1,0)\rangle \\ |X(0,1)\rangle \\ |X(1,1)\rangle \end{pmatrix}. \tag{59}$$

However, the vector $\overline{X(n)}$ consists of the quantum states $|X(0)\rangle, |X(2)\rangle, |X(1)\rangle, |X(3)\rangle$, which are not in numerical order. These indices correspond, in binary form, to the quantum states $|x(0,0)\rangle, |x(0,1)\rangle, |x(1,0)\rangle, |x(1,1)\rangle$.

If the bits of the index $X(n)$ are flipped, the order of the quantum states becomes

$$|x(0,0)\rangle, \quad |x(1,0)\rangle, \quad |x(0,1)\rangle, \quad |x(1,1)\rangle,$$

which corresponds to a bit-reversal permutation.

The transformation at this stage is given by:

$$\begin{aligned} |x_1(0,0)\rangle &= \frac{1}{\sqrt{2}}\left(|x_0(0,0)\rangle + W^0|x_0(1,0)\rangle\right), \\ |x_1(0,1)\rangle &= \frac{1}{\sqrt{2}}\left(|x_0(0,1)\rangle + W^0|x_0(1,1)\rangle\right), \\ |x_1(1,0)\rangle &= \frac{1}{\sqrt{2}}\left(|x_0(0,0)\rangle + W^2|x_0(1,0)\rangle\right), \\ |x_1(1,1)\rangle &= \frac{1}{\sqrt{2}}\left(|x_0(0,1)\rangle + W^2|x_0(1,1)\rangle\right). \end{aligned} \tag{60}$$

In matrix form, this reads:

$$\begin{pmatrix} |x_1(0,0)\rangle \\ |x_1(0,1)\rangle \\ |x_1(1,0)\rangle \\ |x_1(1,1)\rangle \end{pmatrix} = \frac{1}{\sqrt{2}} \begin{pmatrix} 1 & 0 & W^0 & 0 \\ 0 & 1 & 0 & W^0 \\ 1 & 0 & W^2 & 0 \\ 0 & 1 & 0 & W^2 \end{pmatrix} \begin{pmatrix} |x_0(0,0)\rangle \\ |x_0(0,1)\rangle \\ |x_0(1,0)\rangle \\ |x_0(1,1)\rangle \end{pmatrix}. \tag{61}$$

At the second stage, the transformation is:

$$\begin{cases} |x_2(0,0)\rangle = \frac{1}{\sqrt{2}}\left(|x_1(0,0)\rangle + W^0|x_1(0,1)\rangle\right), \\ |x_2(0,1)\rangle = \frac{1}{\sqrt{2}}\left(|x_1(0,0)\rangle + W^2|x_1(0,1)\rangle\right), \\ |x_2(1,0)\rangle = \frac{1}{\sqrt{2}}\left(|x_1(1,0)\rangle + W^1|x_1(1,1)\rangle\right), \\ |x_2(1,1)\rangle = \frac{1}{\sqrt{2}}\left(|x_1(1,0)\rangle + W^3|x_1(1,1)\rangle\right). \end{cases} \tag{62}$$

Its matrix form is:

$$\begin{pmatrix} |x_2(0,0)\rangle \\ |x_2(0,1)\rangle \\ |x_2(1,0)\rangle \\ |x_2(1,1)\rangle \end{pmatrix} = \frac{1}{\sqrt{2}} \begin{pmatrix} 1 & W^0 & 0 & 0 \\ 1 & W^2 & 0 & 0 \\ 0 & 0 & 1 & W^1 \\ 0 & 0 & 1 & W^3 \end{pmatrix} \begin{pmatrix} |x_1(0,0)\rangle \\ |x_1(0,1)\rangle \\ |x_1(1,0)\rangle \\ |x_1(1,1)\rangle \end{pmatrix}. \tag{63}$$

Finally, from Eqs. (59) and (63), the relation

$$|\boldsymbol{X(n_1, n_0)}\rangle = |\boldsymbol{x_2(n_0, n_1)}\rangle \tag{64}$$

shows that the indices in $|X\rangle$ are the bit-reversal of those in $|x_2\rangle$.

B Derivation of Equations for the Matrix Representation of the Two-Qubit System in Subsection 4.1.2

As discussed in **Section 4**, Fig. 4 depicts an OQFT system designed to implement operations on a two-qubit system. The overall system is composed of three main stages:

- **First stage:** two beam splitters labeled α and γ,
- **Second stage:** the waveguide and delay parts,
- **Final stage:** two additional beam splitters, β and κ.

The goal is to compute the final output state of a photon after passing through these three stages.

The transformation after the first stage (beam splitters α and γ) acting on the initial input state vector $\begin{pmatrix} a & b & c & d \end{pmatrix}^T$ is expressed by:

$$\begin{pmatrix} \psi_1 \\ \psi_2 \\ \psi_3 \\ \psi_4 \end{pmatrix} = \begin{pmatrix} \cos\frac{\alpha}{2} & 0 & \sin\frac{\alpha}{2} & 0 \\ \sin\frac{\alpha}{2} & 0 & -\cos\frac{\alpha}{2} & 0 \\ 0 & \cos\frac{\gamma}{2} & 0 & \sin\frac{\gamma}{2} \\ 0 & \sin\frac{\gamma}{2} & 0 & -\cos\frac{\gamma}{2} \end{pmatrix} \begin{pmatrix} a \\ b \\ c \\ d \end{pmatrix} \tag{65}$$

Here, the matrix is block-diagonal and describes independent transformations on two pairs of modes, reflecting the operation of beam splitters α and γ on the corresponding qubit basis states.

Next, the second stage includes a phase shift and two more beam splitters β and κ. The corresponding transformation is:

$$\begin{pmatrix} \psi_{\text{out1}} \\ \psi_{\text{out2}} \\ \psi_{\text{out3}} \\ \psi_{\text{out4}} \end{pmatrix} = \begin{pmatrix} \cos\frac{\beta}{2} & 0 & \sin\frac{\beta}{2} & 0 \\ \sin\frac{\beta}{2} & 0 & -\cos\frac{\beta}{2} & 0 \\ 0 & \cos\frac{\kappa}{2} & 0 & \sin\frac{\kappa}{2} \\ 0 & \sin\frac{\kappa}{2} & 0 & -\cos\frac{\kappa}{2} \end{pmatrix} \begin{pmatrix} 1 & 0 & 0 & 0 \\ 0 & 1 & 0 & 0 \\ 0 & 0 & 1 & 0 \\ 0 & 0 & 0 & e^{\frac{-i\pi}{2}} \end{pmatrix} \begin{pmatrix} \cos\frac{\alpha}{2} & 0 & \sin\frac{\alpha}{2} & 0 \\ \sin\frac{\alpha}{2} & 0 & -\cos\frac{\alpha}{2} & 0 \\ 0 & \cos\frac{\gamma}{2} & 0 & \sin\frac{\gamma}{2} \\ 0 & \sin\frac{\gamma}{2} & 0 & -\cos\frac{\gamma}{2} \end{pmatrix} \begin{pmatrix} a \\ b \\ c \\ d \end{pmatrix} \tag{66}$$

The middle matrix applies a phase shift $e^{-i\pi/2}$ to the last component, representing a phase shifter acting on one mode, which is essential for controlling quantum interference effects in the system.

Multiplying the matrices in Eq. (66) explicitly, the resulting transformation becomes:

$$\begin{pmatrix} \psi_{\text{out1}} \\ \psi_{\text{out2}} \\ \psi_{\text{out3}} \\ \psi_{\text{out4}} \end{pmatrix} = \begin{pmatrix} \cos\frac{\beta}{2} & 0 & \sin\frac{\beta}{2} & 0 \\ \sin\frac{\beta}{2} & 0 & -\cos\frac{\beta}{2} & 0 \\ 0 & \cos\frac{\kappa}{2} & 0 & \sin\frac{\kappa}{2} \\ 0 & \sin\frac{\kappa}{2} & 0 & -\cos\frac{\kappa}{2} \end{pmatrix} \begin{pmatrix} \cos\frac{\alpha}{2} & 0 & \sin\frac{\alpha}{2} & 0 \\ \sin\frac{\alpha}{2} & 0 & -\cos\frac{\alpha}{2} & 0 \\ 0 & \cos\frac{\gamma}{2} & 0 & \sin\frac{\gamma}{2} \\ 0 & e^{\frac{-i\pi}{2}}\sin\frac{\gamma}{2} & 0 & -e^{\frac{-i\pi}{2}}\cos\frac{\gamma}{2} \end{pmatrix} \begin{pmatrix} a \\ b \\ c \\ d \end{pmatrix} \tag{67}$$

This step effectively combines the effects of all three stages into a single matrix multiplication.

After carrying out the matrix multiplications, the final explicit form of the transformation matrix is:

$$\begin{pmatrix} \psi_{\text{out1}} \\ \psi_{\text{out2}} \\ \psi_{\text{out3}} \\ \psi_{\text{out4}} \end{pmatrix} = \begin{pmatrix} \cos\frac{\alpha}{2}\cos\frac{\beta}{2} & \sin\frac{\beta}{2}\cos\frac{\gamma}{2} & \cos\frac{\beta}{2}\sin\frac{\alpha}{2} & \sin\frac{\beta}{2}\sin\frac{\gamma}{2} \\ \sin\frac{\beta}{2}\cos\frac{\alpha}{2} & -\cos\frac{\beta}{2}\cos\frac{\gamma}{2} & \sin\frac{\alpha}{2}\sin\frac{\beta}{2} & -\cos\frac{\beta}{2}\sin\frac{\gamma}{2} \\ \cos\frac{\kappa}{2}\sin\frac{\alpha}{2} & e^{\frac{-i\pi}{2}}\sin\frac{\gamma}{2}\sin\frac{\kappa}{2} & -\cos\frac{\kappa}{2}\cos\frac{\alpha}{2} & -e^{\frac{-i\pi}{2}}\sin\frac{\kappa}{2}\cos\frac{\gamma}{2} \\ \sin\frac{\kappa}{2}\sin\frac{\alpha}{2} & -e^{\frac{-i\pi}{2}}\cos\frac{\kappa}{2}\sin\frac{\gamma}{2} & -\sin\frac{\kappa}{2}\cos\frac{\alpha}{2} & e^{\frac{-i\pi}{2}}\cos\frac{\gamma}{2}\cos\frac{\kappa}{2} \end{pmatrix} \begin{pmatrix} a \\ b \\ c \\ d \end{pmatrix} \tag{68}$$

For clarity, the output amplitudes can also be written explicitly as:

$$\begin{cases} \psi_{\text{out1}} = \cos\frac{\alpha}{2}\cos\frac{\beta}{2}a + \sin\frac{\beta}{2}\cos\frac{\gamma}{2}b + \cos\frac{\beta}{2}\sin\frac{\alpha}{2}c + \sin\frac{\beta}{2}\sin\frac{\gamma}{2}d \\ \psi_{\text{out2}} = \sin\frac{\beta}{2}\cos\frac{\alpha}{2}a - \cos\frac{\beta}{2}\cos\frac{\gamma}{2}b + \sin\frac{\alpha}{2}\sin\frac{\beta}{2}c - \cos\frac{\beta}{2}\sin\frac{\gamma}{2}d \\ \psi_{\text{out3}} = \cos\frac{\kappa}{2}\sin\frac{\alpha}{2}a + e^{\frac{-i\pi}{2}}\sin\frac{\gamma}{2}\sin\frac{\kappa}{2}b - \cos\frac{\kappa}{2}\cos\frac{\alpha}{2}c - e^{\frac{-i\pi}{2}}\sin\frac{\kappa}{2}\cos\frac{\gamma}{2}d \\ \psi_{\text{out4}} = \sin\frac{\kappa}{2}\sin\frac{\alpha}{2}a - e^{\frac{-i\pi}{2}}\cos\frac{\kappa}{2}\sin\frac{\gamma}{2}b - \sin\frac{\kappa}{2}\cos\frac{\alpha}{2}c + e^{\frac{-i\pi}{2}}\cos\frac{\gamma}{2}\cos\frac{\kappa}{2}d \end{cases} \tag{69}$$

This result is consistent with Eq. (19) in the main text, confirming the validity of the derivation.

Finally, by identifying the parameters as $\alpha = \theta_{00}$, $\beta = \theta_{01}$, $\gamma = \theta_{10}$, and $\kappa = \theta_{11}$, the resulting matrix establishes the correspondence between the physical optical implementation and its matrix representation in the quantum gate formalism.

$$\begin{pmatrix} \psi_{out1} \\ \psi_{out2} \\ \psi_{out3} \\ \psi_{out4} \end{pmatrix} = \begin{pmatrix} cos\frac{\theta_{01}}{2} & \sin\frac{\theta_{01}}{2} & 0 & 0 \\ sin\frac{\theta_{01}}{2} & -\cos\frac{\theta_{01}}{2} & 0 & 0 \\ 0 & 0 & cos\frac{\theta_{11}}{2} & e^{\frac{i\pi}{2}}\sin\frac{\theta_{11}}{2} \\ 0 & 0 & sin\frac{\theta_{11}}{2} & e^{\frac{3i\pi}{2}}\cos\frac{\theta_{11}}{2} \end{pmatrix} \begin{pmatrix} cos\frac{\theta_{00}}{2} & 0 & \sin\frac{\theta_{00}}{2} & 0 \\ 0 & cos\frac{\theta_{10}}{2} & 0 & \sin\frac{\theta_{10}}{2} \\ sin\frac{\theta_{00}}{2} & 0 & -\cos\frac{\theta_{00}}{2} & 0 \\ 0 & sin\frac{\theta_{10}}{2} & 0 & -\cos\frac{\theta_{10}}{2} \end{pmatrix} \begin{pmatrix} a \\ b \\ c \\ d \end{pmatrix} \tag{70}$$

$$\begin{pmatrix}\psi_{out1}\\ \psi_{out2}\\ \psi_{out3}\\ \psi_{out4}\end{pmatrix}=\begin{pmatrix} cos\frac{\theta_{01}}{2}cos\frac{\theta_{00}}{2} & \sin\frac{\theta_{01}}{2}cos\frac{\theta_{10}}{2} & cos\frac{\theta_{01}}{2}sin\frac{\theta_{00}}{2} & sin\frac{\theta_{01}}{2}sin\frac{\theta_{10}}{2}\\ sin\frac{\theta_{01}}{2}cos\frac{\theta_{00}}{2} & -\cos\frac{\theta_{01}}{2}cos\frac{\theta_{10}}{2} & sin\frac{\theta_{01}}{2}sin\frac{\theta_{00}}{2} & -cos\frac{\theta_{01}}{2}sin\frac{\theta_{10}}{2}\\ cos\frac{\theta_{11}}{2}cos\frac{\theta_{00}}{2} & e^{\frac{i\pi}{2}}\sin\frac{\theta_{11}}{2}sin\frac{\theta_{10}}{2} & -cos\frac{\theta_{11}}{2}cos\frac{\theta_{00}}{2} & -e^{\frac{i\pi}{2}}\sin\frac{\theta_{11}}{2}cos\frac{\theta_{10}}{2}\\ sin\frac{\theta_{11}}{2}cos\frac{\theta_{00}}{2} & e^{\frac{3i\pi}{2}}\cos\frac{\theta_{11}}{2}sin\frac{\theta_{10}}{2} & -sin\frac{\theta_{11}}{2}cos\frac{\theta_{00}}{2} & -e^{\frac{3i\pi}{2}}\cos\frac{\theta_{11}}{2}cos\frac{\theta_{10}}{2}\end{pmatrix}\begin{pmatrix}a\\ b\\ c\\ d\end{pmatrix} \tag{71}$$

C Derivative of the Equation in Subsection 4.2

By replacing W, introduced in **Section3**, and considering imperfect beam splitters, Eq. (49) becomes:

$$\begin{pmatrix}x_2(0,0,0)\\ x_2(0,0,1)\\ x_2(0,1,0)\\ x_2(0,1,1)\\ x_2(1,0,0)\\ x_2(1,0,1)\\ x_2(1,1,0)\\ x_2(1,1,1)\end{pmatrix}=\begin{pmatrix}\cos\frac{\theta_{02}}{2} & \sin\frac{\theta_{02}}{2} & 0 & 0 & 0 & 0 & 0 & 0\\ \sin\frac{\theta_{02}}{2} & e^{\frac{4\pi}{8}}\cos\frac{\theta_{02}}{2} & 0 & 0 & 0 & 0 & 0 & 0\\ 0 & 0 & \cos\frac{\theta_{12}}{2} & e^{\frac{2\pi}{8}}\sin\frac{\theta_{12}}{2} & 0 & 0 & 0 & 0\\ 0 & 0 & \sin\frac{\theta_{12}}{2} & e^{\frac{6\pi}{8}}\cos\frac{\theta_{12}}{2} & 0 & 0 & 0 & 0\\ 0 & 0 & 0 & 0 & \cos\frac{\theta_{22}}{2} & e^{\frac{1\pi}{8}}\sin\frac{\theta_{22}}{2} & 0 & 0\\ 0 & 0 & 0 & 0 & \sin\frac{\theta_{22}}{2} & e^{\frac{5\pi}{8}}\cos\frac{\theta_{22}}{2} & 0 & 0\\ 0 & 0 & 0 & 0 & 0 & 0 & \cos\frac{\theta_{32}}{2} & e^{\frac{3\pi}{8}}\sin\frac{\theta_{32}}{2}\\ 0 & 0 & 0 & 0 & 0 & 0 & \sin\frac{\theta_{32}}{2} & e^{\frac{7\pi}{8}}\cos\frac{\theta_{32}}{2}\end{pmatrix}$$
$$\begin{pmatrix}\cos\frac{\theta_{01}}{2} & 0 & \sin\frac{\theta_{01}}{2} & 0 & 0 & 0 & 0 & 0\\ 0 & \cos\frac{\theta_{11}}{2} & 0 & \sin\frac{\theta_{11}}{2} & 0 & 0 & 0 & 0\\ \sin\frac{\theta_{01}}{2} & 0 & e^{\frac{8\pi}{8}}\cos\frac{\theta_{01}}{2} & 0 & 0 & 0 & 0 & 0\\ 0 & \sin\frac{\theta_{11}}{2} & 0 & e^{\frac{8\pi}{8}}\cos\frac{\theta_{11}}{2} & 0 & 0 & 0 & 0\\ 0 & 0 & 0 & 0 & \cos\frac{\theta_{21}}{2} & 0 & e^{\frac{4\pi}{8}}\sin\frac{\theta_{21}}{2} & 0\\ 0 & 0 & 0 & 0 & 0 & \cos\frac{\theta_{31}}{2} & 0 & e^{\frac{4\pi}{8}}\sin\frac{\theta_{31}}{2}\\ 0 & 0 & 0 & 0 & \sin\frac{\theta_{21}}{2} & 0 & e^{\frac{12\pi}{8}}cos\frac{\theta_{21}}{2} & 0\\ 0 & 0 & 0 & 0 & 0 & \sin\frac{\theta_{31}}{2} & 0 & e^{\frac{12\pi}{8}}\cos\frac{\theta_{31}}{2}\end{pmatrix}$$
$$\begin{pmatrix}\cos\frac{\theta_{00}}{2} & 0 & 0 & 0 & \sin\frac{\theta_{00}}{2} & 0 & 0 & 0\\ 0 & \cos\frac{\theta_{10}}{2} & 0 & 0 & 0 & \sin\frac{\theta_{10}}{2} & 0 & 0\\ 0 & 0 & \cos\frac{\theta_{20}}{2} & 0 & 0 & 0 & \sin\frac{\theta_{20}}{2} & 0\\ 0 & 0 & 0 & \cos\frac{\theta_{30}}{2} & 0 & 0 & 0 & \sin\frac{\theta_{30}}{2}\\ \sin\frac{\theta_{00}}{2} & 0 & 0 & 0 & -\cos\frac{\theta_{00}}{2} & 0 & 0 & 0\\ 0 & \sin\frac{\theta_{10}}{2} & 0 & 0 & 0 & -\cos\frac{\theta_{10}}{2} & 0 & 0\\ 0 & 0 & \sin\frac{\theta_{20}}{2} & 0 & 0 & 0 & -\cos\frac{\theta_{20}}{2} & 0\\ 0 & 0 & 0 & \sin\frac{\theta_{30}}{2} & 0 & 0 & 0 & -\cos\frac{\theta_{30}}{2}\end{pmatrix}\begin{pmatrix}x_0(0,0,0)\\ x_0(0,0,1)\\ x_0(0,1,0)\\ x_0(0,1,1)\\ x_0(1,0,0)\\ x_0(1,0,1)\\ x_0(1,1,0)\\ x_0(1,1,1)\end{pmatrix} \tag{72}$$

This equation represents the state evolution of a three-qubit quantum system under imperfect beam splitter operations and phase shifts. Here, each matrix corresponds to one stage of the transformation:

- The first matrix accounts for beam splitter imperfections and associated phase factors parameterized by θ_{i2}.
- The second matrix similarly models beam splitter effects with parameters θ_{i1}, including phase terms due to delay lines or waveguide lengths.
- The third matrix includes additional unitary rotations and reflections characterized by θ_{i0}, representing the final beam splitter imperfections or phase shifters.

Each element in the state vectors $x_j(\cdot)$ corresponds to a specific computational basis state labeled by the three-bit index (b_2, b_1, b_0). The exponential factors $e^{i\phi}$ represent phase shifts arising from path differences and delays, while the sine and cosine terms arise from the imperfect splitting ratios of the beam splitters.

This decomposition allows the full system operation to be described as a product of these unitary matrices acting sequentially on the initial quantum state vector.

Statements and declarations

- **Data Availability**: The data generated and/or analysed during the current study are available from the corresponding author on reasonable request.
- **Conflict of Interest**: Authors state no conflict of interest.
- **Funding**: No funding was received to assist with the preparation of this manuscript.

References

[1] Feynman, R.P.: Simulating physics with computers. *Int. J. Theor. Phys.* **21**(6/7), 467–488 (1982)

[2] Bruzewicz, C.D., Chiaverini, J., McConnell, R., Sage, J.M.: Trapped-ion quantum computing: progress and challenges. *Appl. Phys. Rev.* **6**(2), 021314 (2019)

[3] Kjaergaard, M., Schwartz, M.E., Braumüller, J., Krantz, P., Wang, J.I.-J., Gustavsson, S., Oliver, W.D.: Superconducting qubits: current state of play. *Annu. Rev. Condens. Matter Phys.* **11**, 369–395 (2020)

[4] O'Brien, J.L., Furusawa, A., Vučković, J.: Photonic quantum technologies. *Nat. Photon.* **3**(12), 687–695 (2009)

[5] Knill, E., Laflamme, R., Milburn, G.J.: A scheme for efficient quantum computation with linear optics. *Nature* **409**(6816), 46–52 (2001)

[6] Wang, J., Sciarrino, F., Laing, A., Thompson, M.G.: Integrated photonic quantum technologies. *Nat. Photon.* **14**(5), 273–284 (2020)

[7] Reck, M., Zeilinger, A., Bernstein, H.J., Bertani, P.: Experimental realization of any discrete unitary operator. *Phys. Rev. Lett.* **73**(1), 58–61 (1994)

[8] Politi, A., Matthews, J.C.F., O'Brien, J.L.: Silica-on-silicon waveguide quantum circuits. *Science* **320**(5876), 646–649 (2008)

[9] Shor, P.W.: Polynomial-time algorithms for prime factorization and discrete logarithms on a quantum computer. *SIAM Rev.* **41**(2), 303–332 (1999)

[10] Nielsen, M.A., Chuang, I.L.: *Quantum Computation and Quantum Information*, 10th edn. Cambridge University Press, Cambridge (2010)

[11] Barenco, A., Bennett, C.H., Cleve, R., DiVincenzo, D.P., Margolus, N., Shor, P., et al.: Elementary gates for quantum computation. *Phys. Rev. A* **52**(5), 3457–3467 (1996)

[12] Tabia, G.N.M.: Recursive multiport schemes for implementing quantum algorithms with photonic integrated circuits. *Phys. Rev. A* **93**(1), 012323 (2016)

[13] Chu, D.C.: Inside the discrete Fourier transform. *IEEE Trans. Signal Process.* **47**(7), 1839–1850 (1999)

[14] Brigham, E.O.: *The Fast Fourier Transform and Its Applications*. Prentice-Hall, Englewood Cliffs (1988)

[15] Barak, R., Ben-Aryeh, Y.: Quantum fast Fourier transform and quantum computation by linear optics. *J. Opt. Soc. Am. B* **24**(2), 231–240 (2007)

[16] Cooley, J.W., Tukey, J.W.: An algorithm for the machine calculation of complex Fourier series. *Math. Comput.* **19**(90), 297–301 (1965)

[17] Brigham, E.O.: *The Fast Fourier Transform and Its Applications*. Prentice-Hall, Englewood Cliffs (1988)

[18] Nielsen, M.A., Chuang, I.L.: *Quantum Computation and Quantum Information*, 10th edn. Cambridge University Press, Cambridge (2010)

[19] Shor, P.W.: Algorithms for quantum computation: discrete logarithms and factoring. In: *Proceedings 35th Annual Symposium on Foundations of Computer Science*, pp. 124–134. IEEE (1994)

[20] Griffiths, R.B., Niu, C.-S.: Semiclassical Fourier transform for quantum computation. *arXiv preprint* quant-ph/9511007 (1995). https://arxiv.org/abs/quant-ph/9511007

[21] Cleve, R., Ekert, A., Macchiavello, C., Mosca, M.: Quantum algorithms revisited. *Proc. R. Soc. Lond. A* **454**(1969), 339–354 (1998)

[22] Myers, C.R., Laflamme, R.: Linear optics quantum computation: an overview. In: *Quantum Computers, Algorithms and Chaos*, pp. 45–93. IOS Press (2006)

[23] Hénault, F.: Quantum physics and the beam splitter mystery. In: *The Nature of Light: What are Photons? VI*, vol. 9570, pp. 199–213. SPIE (2015)

[24] Törmä, P., Jex, I., Stenholm, S.: Beam splitter realizations of totally symmetric mode couplers. *J. Mod. Opt.* **43**(2), 245–251 (1996)

[25] Takeuchi, S.: Analysis of errors in linear-optics quantum computation. *Phys. Rev. A* **61**(5), 052302 (2000)

[26] Zeilinger, A.: General properties of lossless beam splitters in interferometry. *Am. J. Phys.* **49**(9), 882–883 (1981)

[27] Degiorgio, V.: Phase shift between the transmitted and the reflected optical fields of a semireflecting lossless mirror. *Am. J. Phys.* **48**(1), 81 (1980)

[28] Cerf, N.J., Adami, C., Kwiat, P.G.: Optical simulation of quantum logic. *Phys. Rev. A* **57**(3), R1477–R1480 (1998)

[29] Leonhardt, U., Paul, H.: Measuring the quantum state of light. *Prog. Quantum Electron.* **19**(2), 89–130 (1995)

[30] Brigham, E.O.: *The Fast Fourier Transform*. Prentice-Hall, Englewood Cliffs (1974)

[31] Laing, A., Lawson, T., Martin Lopez, E., O'Brien, J.L.: Observation of quantum interference as a function of Berry's phase in a complex Hadamard optical network. *Phys. Rev. Lett.* **108**(26), 260505 (2012)

[32] Żukowski, M., Zeilinger, A., Horne, M.A.: Realizable higher-dimensional two-particle entanglements via multiport beam splitters. *Phys. Rev. A* **55**(4), 2564–2579 (1997)

[33] Paesani, S., Bulmer, J.F.F., Jones, A.E., Santagati, R., Laing, A.: Scheme for universal high-dimensional quantum computation with linear optics. *Phys. Rev. Lett.* **126**(23), 230504 (2021)

[34] Jin, R.-B., Zeng, Z.-Q., You, C., Yuan, C.: Quantum interferometers: principles and applications. *Prog. Quantum Electron.* 100519 (2024)

[35] Clements, W.R., Humphreys, P.C., Metcalf, B.J., Kolthammer, W.S., Walmsley, I.A.: Optimal design for universal multiport interferometers. *Optica* **3**(12), 1460–1465 (2016)

[36] Kok, P., Munro, W.J., Nemoto, K., Ralph, T.C., Dowling, J.P., Milburn, G.J.: Linear optical quantum computing with photonic qubits. *Rev. Mod. Phys.* **79**(1), 135–174 (2007)

[37] Politi, A., Cryan, M.J., Rarity, J.G., Yu, S., O'Brien, J.L.: Silica-on-silicon waveguide quantum circuits. *Science* **320**(5876), 646–649 (2008)

[38] Chen, Y., Ecker, S., Wengerowsky, S., Bulla, L., Joshi, S.K., Steinlechner, F., Ursin, R.: Polarization entanglement by time-reversed Hong–Ou–Mandel interference. *Phys. Rev. Lett.* **121**(20), 200502 (2018)

[39] Aaronson, S., Arkhipov, A.: The computational complexity of linear optics. In: *Proc. 43rd Annu. ACM Symp. Theory Comput.*, pp. 333–342 (2011)

[40] Aspect, A., Dalibard, J., Roger, G.: Experimental test of Bell's inequalities using time-varying analyzers. *Phys. Rev. Lett.* **49**(25), 1804–1807 (1982)

[41] Ataman, S.: A graphical method in quantum optics. *J. Phys. Commun.* **2**(3), 035032 (2018)

[42] Loughridge, R., Abramovitch, D.Y.: A tutorial on laser interferometry for precision measurements. In: *2013 American Control Conference*, pp. 3686–3703. IEEE (2013)

[43] Kalamidas, D.: Feasible quantum error detection with linear optics. *Phys. Lett. A* **321**(2), 87–93 (2004)

[44] Howell, J.C., Yeazell, J.A.: Linear optics simulations of the quantum baker's map. *Phys. Rev. A* **61**(1), 012304 (1999)

[45] Kok, P., Munro, W.J., Nemoto, K., Ralph, T.C., Dowling, J.P., Milburn, G.J.: Linear optical quantum computing. *Rev. Mod. Phys.* **79**(1), 135–174 (2007)

[46] Cho, S.: *Quantum Computation and Quantum Information Simulation Using Python: A Gentle Introduction*. IOP Publishing, Bristol (2022)

[47] Adami, C., Cerf, N.J.: Quantum computation with linear optics. In: *NASA International Conference on Quantum Computing and Quantum Communications*, pp. 391–401. Springer (1998)

[48] Leonhardt, U.: *Measuring the Quantum State of Light*. Cambridge University Press, Cambridge (1997)